Calculations and Mapping of the Magnetic Field in the Prototype Horn 1

(Tasks D and E Report of the Accord between FNAL and IHEP)

A.Abramov, S.Filippov, V.Garkusha, F.Novoskoltsev,
A.Ryabov, A.Shalunov, A.Tikhov, V.Zarucheisky

Contents

1 Introduction

An accurate knowledge of the magnetic field in focusing horns is needed to predict the neutrino beam spectrum in the far detector in the absence of oscillations (using good statistical measurements of the spectrum in the near detector and calculated FAR/NEAR ratio of neutrino spectra). From this point of view and taking also into account a noticeable difference between the final engineering and original beam optics design of horns, the detailed study of the magnetic field in real horns was defined as an important part of the beam design.

This Report is dedicated to results of calculations and measurements of the magnetic field in the prototype of the Horn 1, which were performed under the terms of the 2000 Accord between FNAL and IHEP, in particular:

- Results of calculations of the magnetic field of the prototype horn are presented in the **Section 2**. These results, which were obtained with help of the ANSYS code, include the effects of water spray holes in the outer conductor, local strip-line connections and construction imperfection of the inner conductor.

- **Section 3** gives a brief description of the magnetic measurement hardware, designed and constructed in the IHEP for mapping the magnetic field of the prototype horn. This hardware uses Hall probes as the element sensitive to the magnetic field and is intended for measurements of the focusing field in the neck region and the field induced in the vicinity of the horn axis due to variation of the thickness in the inner conductor.

- Using the hardware described in the Section 3, the real magnetic measurements of the prototype horn were carried out in October 2000 at the FNAL. **Section 4** presents results of these measurements, as well as a comparison of the measured magnetic field with the expected horn field and with results of ANSYS calculations given in the Section 2.

2 Calculations of the Magnetic Field of the Horn 1

This Section presents results of calculations of the magnetic field in the first horn. To study the influence of water spray and drain holes in the outer conductor and local strip-line connections, as well as construction imperfection (eccentricity) of the inner conductor, needed calculations were made for some separate parts of the horn, using the ANSYS code.

Taking into account that the horn will mainly operate with a 2.6 ms pulse for MINOS data-taking (not excluding a 5.2 ms pulse for eventual resonant extraction) and that horn pulses using the test supply are about 0.8 ms, results of the magnetic field calculations for both infinite (the direct current) and 0.8 ms pulse show also the influence of a pulse duration.

It was assumed that the specific resistance ρ_e of the inner conductor material (6061 Al alloy) is equal to 5.1×10^{-8} Ohm·m[1] and that the current varies within the pulse as $I = 200 \sin(\pi t / \tau)$ kA, where τ is the duration of a current pulse.

2.1 Magnetic Field in the vicinity of Spray Holes in the Outer Conductor

The outer conductor of the first horn contains a lot of holes located along three lines, which are parallel to the horn axis and equally spaced by its azimuth. There are 18 holes in each line, where 15 of them $\sim$1.43 cm in diameter are intended for water spray cooling of the inner conductor, while other 3 (1.27 cm in diameter) are used for spider supports. According to a horn design, the distance between axes of neighbouring holes varies from $\sim$7.5 cm to 25.4 cm, i.e. is at least 10 times larger than the radius of a hole. To study the influence of holes in the outer conductor to the focusing magnetic field in the region between the inner and outer conductor, calculations were made for the 1.27 cm diameter single hole (see Figure 2.1).

Results of calculations are given in Figure 2.2, which shows deviations of the toroidal magnetic field from its nominal value $B_0 = \mu_0 I / 2\pi R$ near the hole both for the infinite and 0.8 ms pulse duration. In addition Figure 2.3 shows the behaviour of the B_r component of the field arising in this region simultaneously with a deviation of the main component. As it follows from these Figures:

---

[1]Aluminum Alloys and Products Forms, A.Wehmann's FAX from April 4, 2000.

- the sizes of the area where deviation of the focusing magnetic field from its nominal value is greater than 2% do not exceed $(2.0\text{--}2.5)r$ in the longitudinal (Z) and both transverse (L and R) directions (starting from the center of the hole at the inner surface of the outer conductor) and slightly depend on the pulse duration of a feeding current.

- because of the concentration of the current at the inner surface of the outer conductor, the decrease of the focusing field in the hole axis is more considerable at the short duration of a feeding current pulse. Due to the same reason the magnetic field inside the hole is smaller for the 0.8 ms pulse duration than that for the infinite pulse (see also Figure 2.4).

Taking into account these results and previous results of the neutrino beam simulations for various configurations of the PH2 focusing system[2], one can expect the negligible influence of holes in the outer conductor on neutrino beam parameters, i.e. the magnetic field of the first horn in the layer between $R_{in}^{OC} - 3r$ and R_{in}^{OC} influences only on a few of secondaries, contributing in the neutrino event rate in the detector. Moreover, the magnetic field only in ~10% of the cross-section area of this layer, has more than 2% deviation from its nominal value.

2.2 Deviation of the Magnetic Field due to the Eccentricity of the Inner Conductor

The eccentricity of the inner conductor (mutual displacement of its inner and outer surfaces) generates the dipole field inside the inner conductor, as well as a deviation of the toroidal focusing field from its nominal value outside the inner conductor. Carrying out M.C. simulations of the influence of an eccentricity on the FAR/NEAR ratio, we assumed that the magnetic field at the each point inside and outside the inner conductor may be defined as superposition of magnetic fields produced by two currents of invariable density $j = I/\pi((R_{out}^{IC})^2 - (R_{in}^{IC})^2)$ flowing in opposite directions along infinite cylindrical conductors. In this case for the eccentricity δ in the vertical direction (Figure 2.5) the magnetic fields inside and outside the inner conductor are:

---

[2]See Figures 2.1–2.3 of Task A Report of the Accord between FNAL and IHEP "The PH2M Two Horns Focusing System for the NuMI Project", NuMI-B-471, February 15, 1999.

$$B_x = \frac{\mu_0 I}{2\pi} \frac{\delta}{(R_{out}^{IC})^2 - (R_{in}^{IC})^2}, \qquad (1)$$

$$B_\varphi \simeq B_0 - \Delta B \sin\varphi, \qquad B_r \simeq \Delta B \cos\varphi, \qquad (2)$$

where: $B_0 = \frac{\mu_0 I}{2\pi} \frac{1}{R}$ is the nominal magnetic field in the region between the inner and outer conductor and $\Delta B = \frac{\mu_0 I}{2\pi} \frac{(R_{in}^{IC})^2}{(R_{out}^{IC})^2 - (R_{in}^{IC})^2} \frac{\delta}{R^2}$.

Simulations of the neutrino beam have shown, that the dipole field, arising in the magnetic field free region in case of the ideal conductor, gives the main contribution ($\sim$85%) to changing of the FAR/NEAR ratio due to eccentricity of an inner conductor. The influence of this imperfection in the construction on beam parameters grows with increasing of the neutrino beam energy, i.e. the invariable along the length eccentricity of the inner conductor in the Horn 1 equal to 0.08 mm, causes 2% changing of the FAR/NEAR ratio in case of the LE beam, while corresponding value of an allowable eccentricity for the ME beam is equal to 0.035 mm.

One should note, that construction tolerances obtained for invariable density of the feeding current would be weakened with decreasing of the pulse duration and, consequently, of the skin depth. Calculations of the magnetic field in the central part of the inner conductor of the Horn 1 confirm it. The geometry of the central part of the inner conductor of the Horn 1 is given in Table 2.1.

Z, cm	53.77—77.00	77.00—80.98	80.98—92.13	92.13—104.42
R_{in}^{IC}, cm	$\sqrt{\frac{82.71-Z}{7.048}}$	0.90	$\sqrt{\frac{Z-79.21}{2.185}}$	$\sqrt{\frac{Z-77.00}{2.185}} - 0.2$
R_{out}^{IC}, cm	$\sqrt{\frac{89.85-Z}{7.048}}$	1.35	$\sqrt{\frac{Z-77.00}{2.185}}$	

Table 2.1: The geometry of the central part of the Horn 1 inner conductor.

Results of calculations of the magnetic field inside and outside the inner conductor are given in Figures 2.6–2.9.

Figure 2.8 shows the longitudinal distribution of the dipole magnetic field induced inside the inner conductor due to its 0.1 mm eccentricity in the vertical direction. The distribution of the field for infinite duration of the pulse shows well the variation of the inner conductor cross-section

along the length, i.e. $B_x \simeq 390$ Gs within the region where the cross-section is invariable and then decreases with increasing of the cross-section at $Z \geq 92.13$ cm. Slight difference of the magnetic field at $Z \simeq 79$ cm from the value obtained by (1) may be explained to a variable degree by the calculation accuracy and some features of the distribution of the current density in the neck region even for infinite duration of the pulse (Figure 2.6).

For 2.6 ms and 0.8 ms current pulses the magnetic field inside the inner conductor reaches at the neck values $\sim$300 Gs and $\sim$170 Gs respectively, and then decreases in both directions along the horn length. The analysis of these results permits to make the following estimation for the magnetic field inside the inner conductor for finite duration of the pulse:

$$(B_x)_\tau \simeq (B_x)_\infty \left(1 - \exp(-\frac{s^2}{\Delta R \, R_{in}^{IC}}) \right), \qquad (3)$$

where: $(B_x)_\infty$ is the magnetic field for the infinite pulse duration (1), ΔR is the thickness of the inner conductor, $s \propto \sqrt{\tau \rho_e}$ is the skin depth, τ is the duration of a current pulse and ρ_e is the specific resistance of an inner conductor material.

Figure 2.9 shows deviations of the magnetic field in the region between the inner and outer conductor from the nominal field B_0 due to the 0.1 mm eccentricity of the inner conductor. Results are given for two characteristic cross-sections of the central part of the inner conductor:

- at the neck region ($Z = 79.0$ cm) with the maximal thickness equal to 0.45 cm, where the density of the 0.8 ms pulsed current varies from 55 kA/cm^2 near the inner surface to 71 kA/cm^2 near the outer surface (see Figure 2.7);

- at the downstream end ($Z = 99.1$ cm) with the minimal thickness 0.2 cm, where the density of a pulsed current $\sim$52 kA/cm^2 weakly depends on the radius.

As it follows from these plots, in the second considered cross-section there are no difference between variations of $(B_\varphi - B_0)/B_0$ and B_r/B_0 with radius in two transverse directions, as well as between results obtained with a help of the ANSYS and from expression (2) for the infinite pulse duration. The diametrally opposite situation takes place for the neck region of the inner conductor, which (as in the case of B_x) may be explained by more

complicated distribution of a current density in this cross-section of the conductor and partially by the calculation accuracy.

It was significant to note, that in both cross-sections the deviation of the magnetic field in the region between the inner and outer conductor even somewhat faster than the field inside the inner conductor (B_x) decreases with decreasing of a pulse duration. It means that the dipole field inside the inner conductor remains the determinative factor of the inner conductor eccentricity influence on neutrino beam parameters.

2.3 Magnetic Field in the Downstream Part of the Horn 1

The length of the first horn in its original beam optics design is equal to 3 m. The real length of the prototype horn is about 3.35 m including approximately 0.3 m length of the downstream part with four water drains and strip-line connections. Taking into account that the magnetic field in this region could be substantially different from the uniform toroidal field used in previous neutrino beam simulations, this Subsection presents results of magnetic field calculations for the $\sim$0.5 m length downstream part of the first horn. Calculations were made for the 1/8 azimuthal part ($0 \leq \varphi \leq 45°$) of the horn so that $\varphi = 0°$ corresponds to the center of a water drain hole (see Figures 2.10 and 2.11).

Results of calculations given in Figures 2.12a and 2.12b show, that the non-uniformity of a focusing magnetic field reaches 15–20% near strip-line connections and decreases with increasing of a distance from the downstream flange of the inner conductor, thus the equalization of the field in the azimuthal direction is more rapid for the short current pulse than for the direct current. In both cases four water drain holes form a significant hindrance to the equalization of the magnetic field. The relatively large radius of these holes[3] and, correspondingly, the size of the region between the inner and outer conductor with more than 2% deviation of the magnetic field from the uniform toroidal field gives grounds to take into account these results in neutrino beam simulations.

---

[3]The ratio of the water drain radius to the internal radius of the outer conductor r/R_{in}^{OC} is equal to $\sim$0.34. For comparison, the same parameter for water spray holes is only about 0.043.
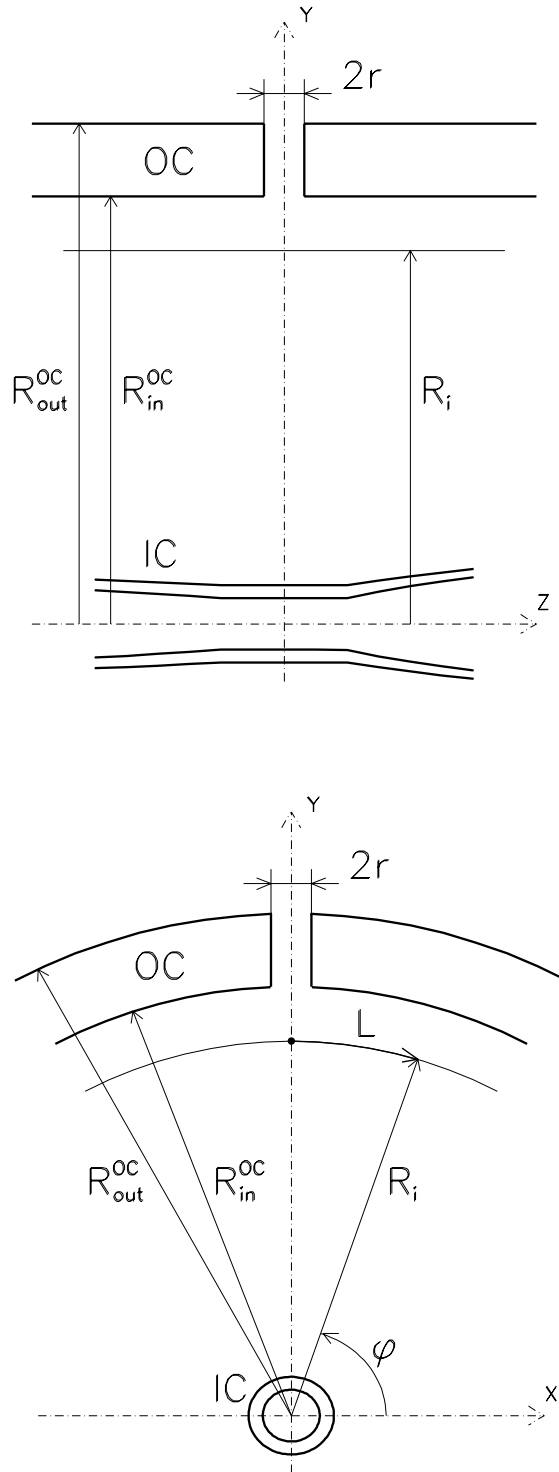
Figure 2.1: To calculations of the magnetic field near the hole in the horn outer conductor. $R_{out}^{OC} = 17.4625$ cm, $R_{in}^{OC} = 14.9225$ cm, $r = 0.635$ cm.
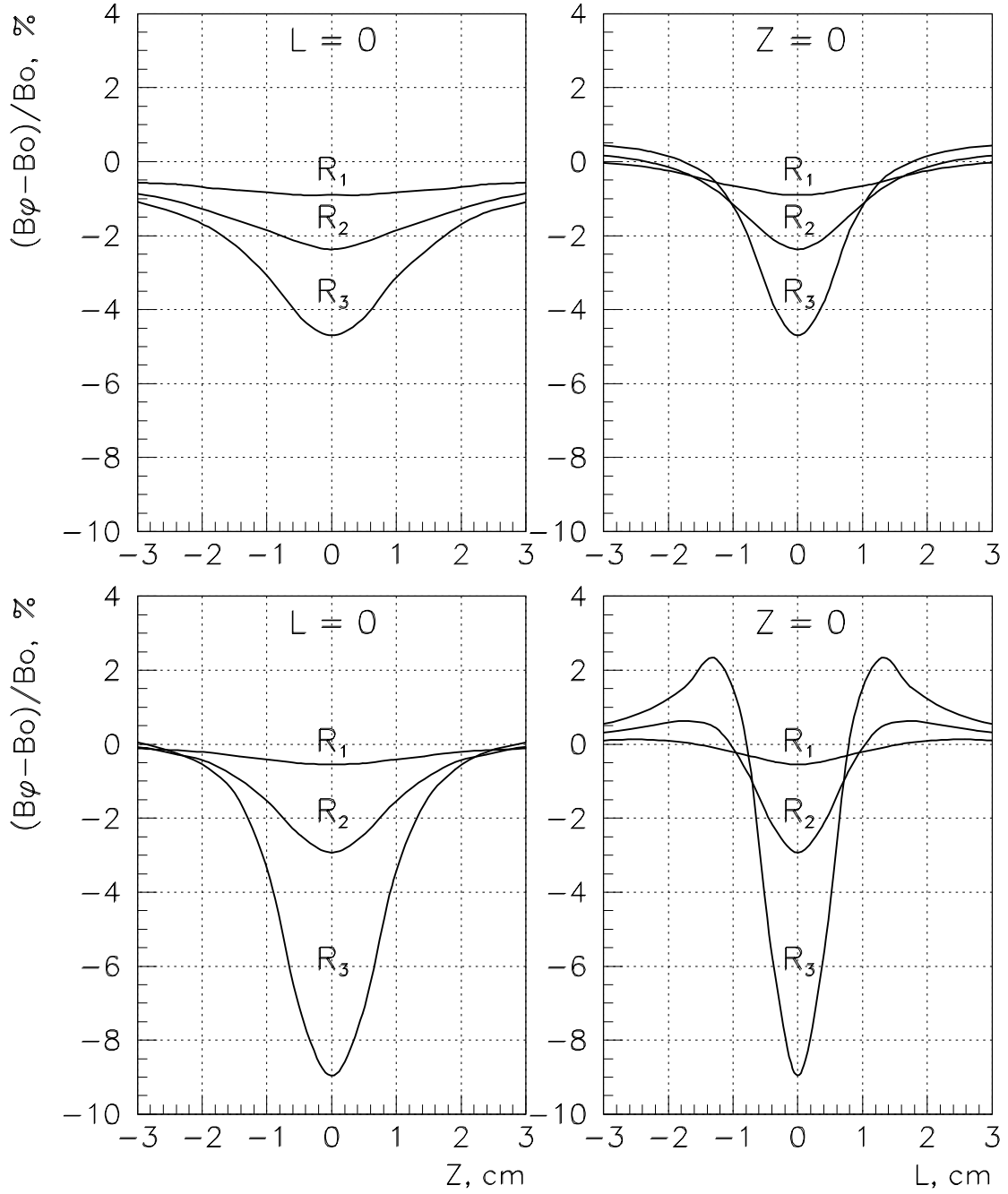
Figure 2.2: Deviations of the toroidal magnetic field B_φ from its nominal value B_0 near the hole in the outer conductor for the infinite (top) and 0.8 ms (bottom) pulse duration of a feeding current.

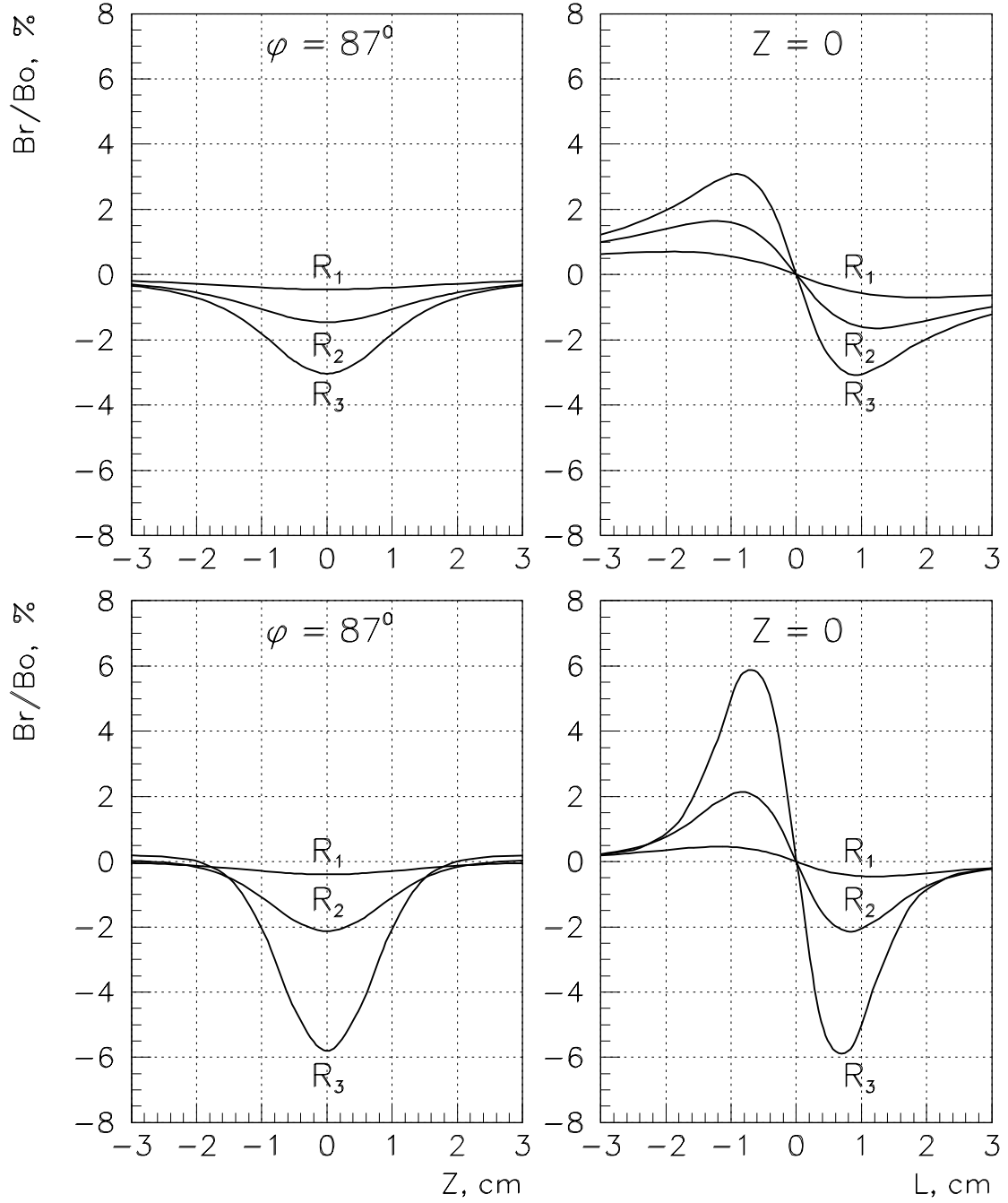$$R_1 = R_{in}^{OC} - 3r, \quad R_2 = R_{in}^{OC} - 1.5r, \quad R_3 = R_{in}^{OC} - 0.75r.$$

Figure 2.3: The behaviour of the B_r component of magnetic field near the hole in the outer conductor for the infinite (top) and 0.8 ms (bottom) pulse duration of a feeding current. $\varphi = 87°$ approximately corresponds to the edge of a hole (Figure 2.1).

$$R_1 = R_{in}^{OC} - 3r, \quad R_2 = R_{in}^{OC} - 1.5r, \quad R_3 = R_{in}^{OC} - 0.75r.$$
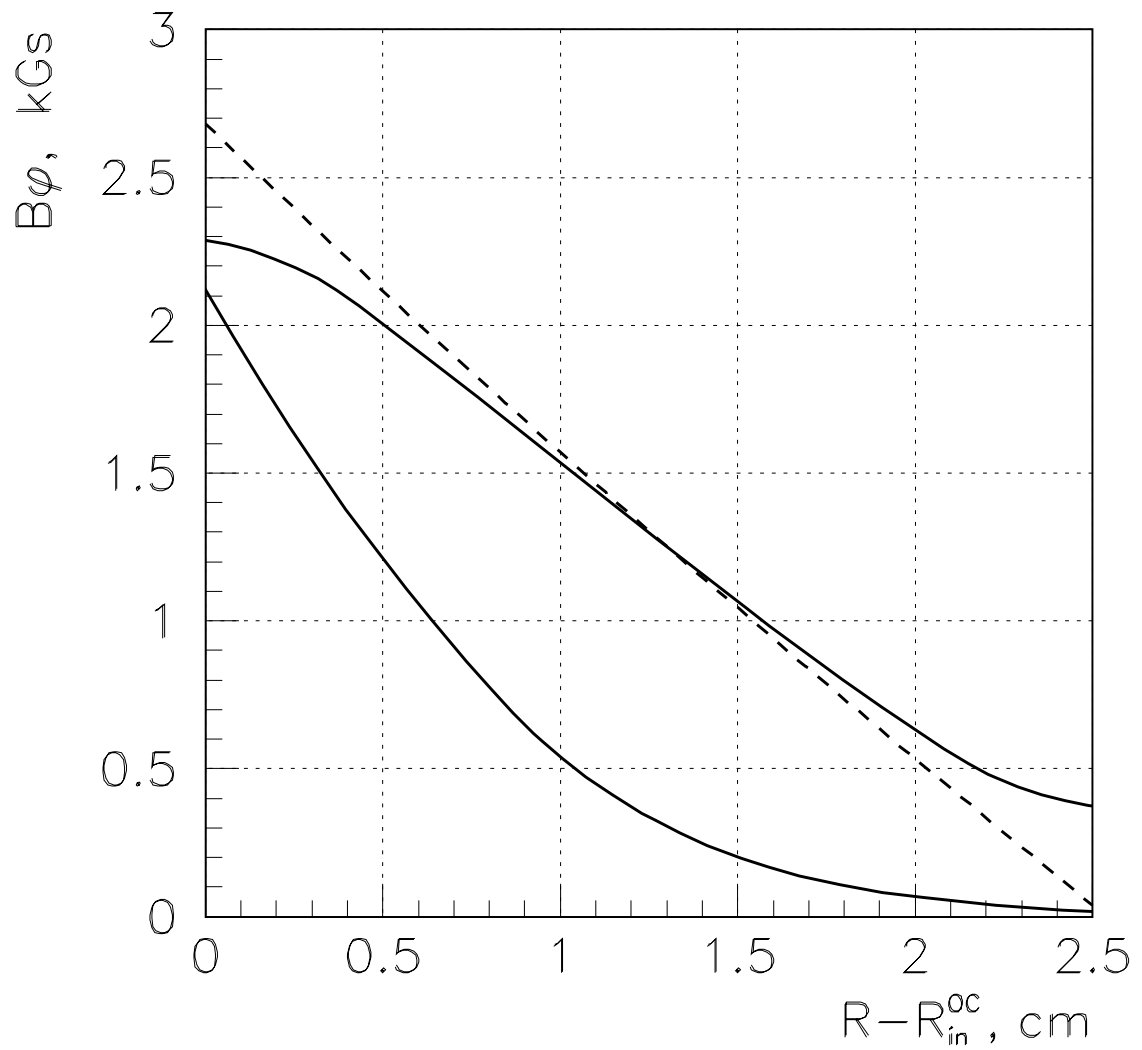
Figure 2.4: The magnetic field at the axis of hole in the outer conductor for the infinite (upper line) and 0.8 ms (lower line) pulse duration of a feeding current. The dashed line shows the magnetic field inside the solid outer conductor for the infinite pulse duration.
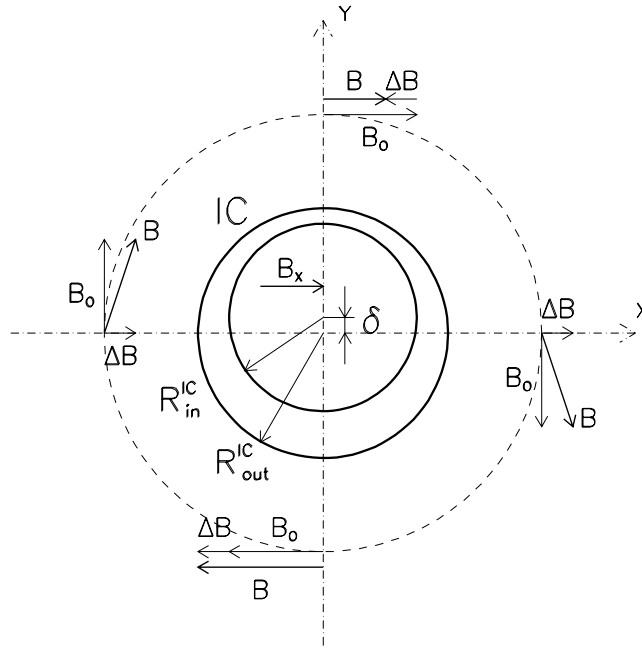
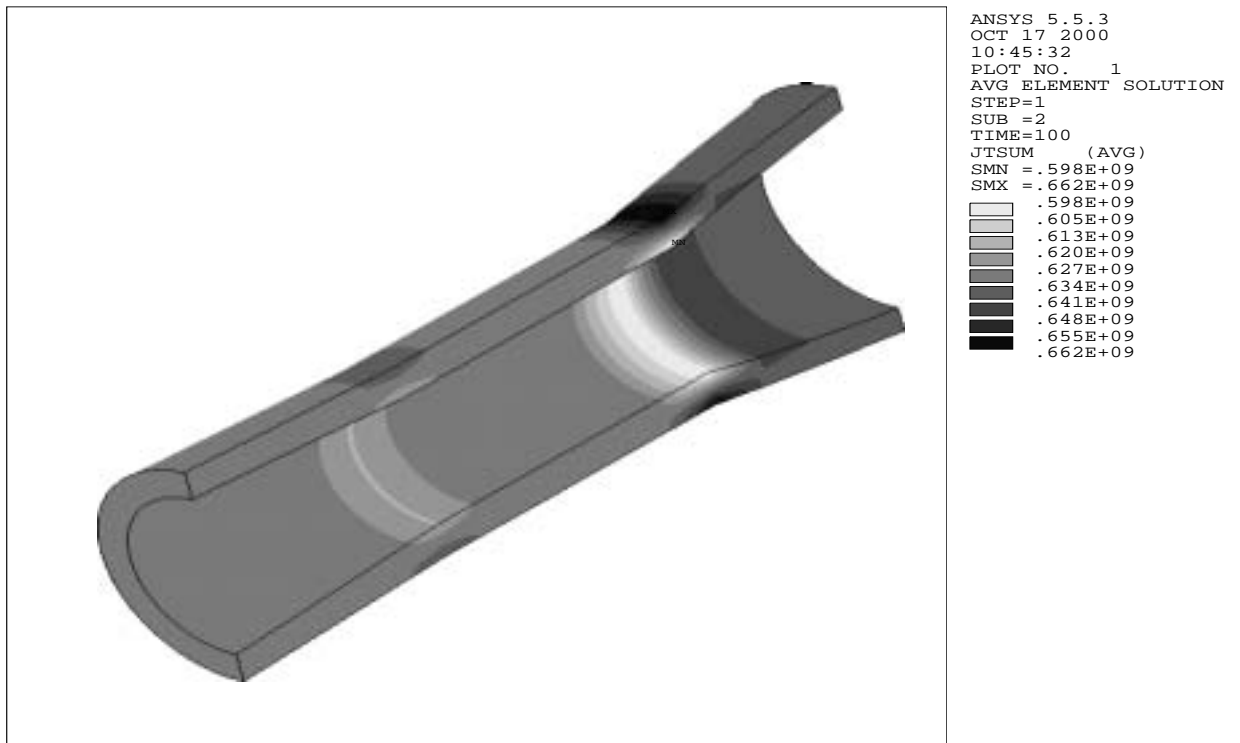Figure 2.5: To calculations of the magnetic field in case of the eccentricity of the inner conductor.

Figure 2.6: The distribution of the direct current density in the neck region of the ideal inner conductor.
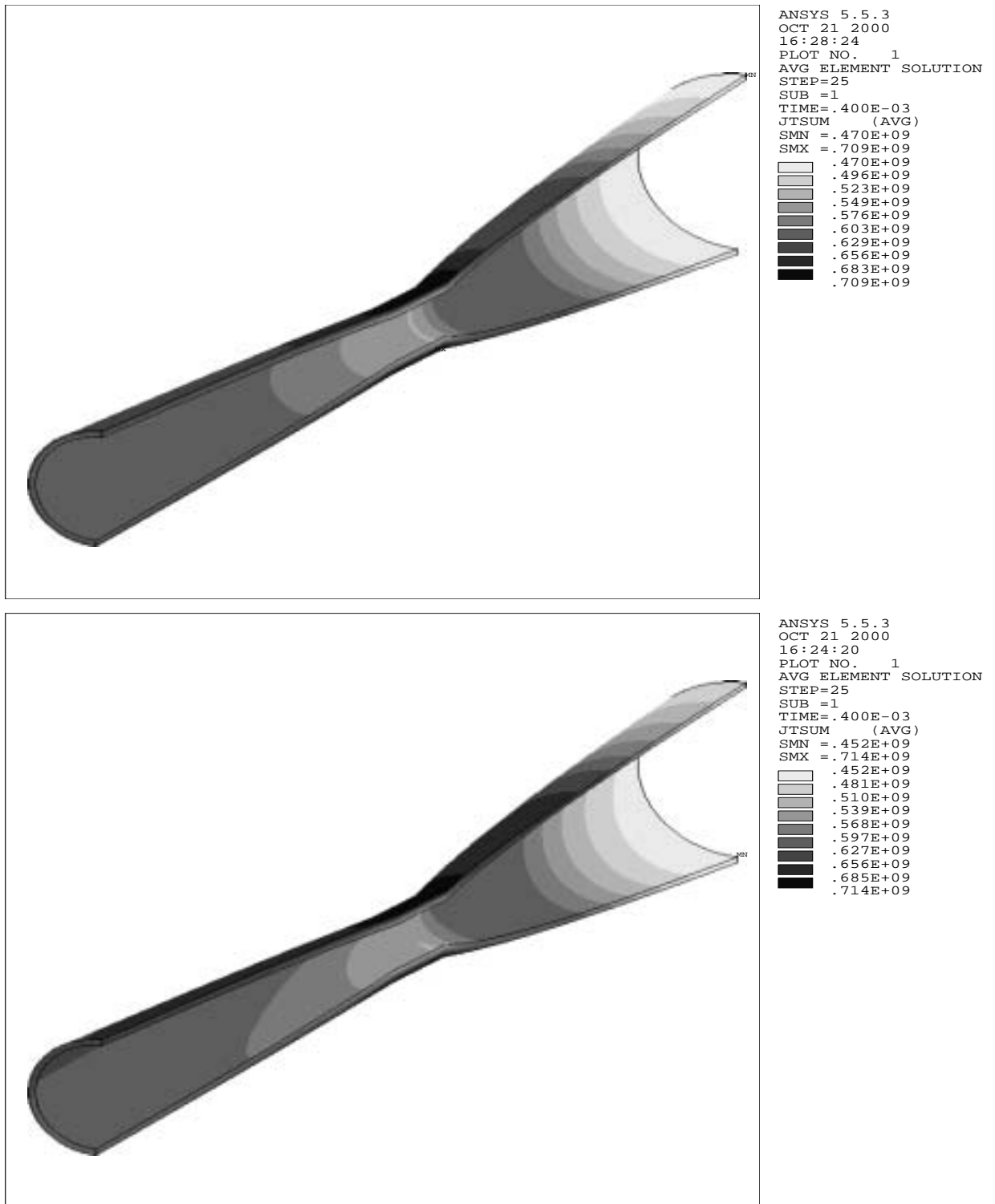
Figure 2.7: Distributions of a density of the 0.8 ms pulse current in the central part of the ideal inner conductor (top) and the inner conductor with the 0.1 mm eccentricity in the vertical direction (bottom).
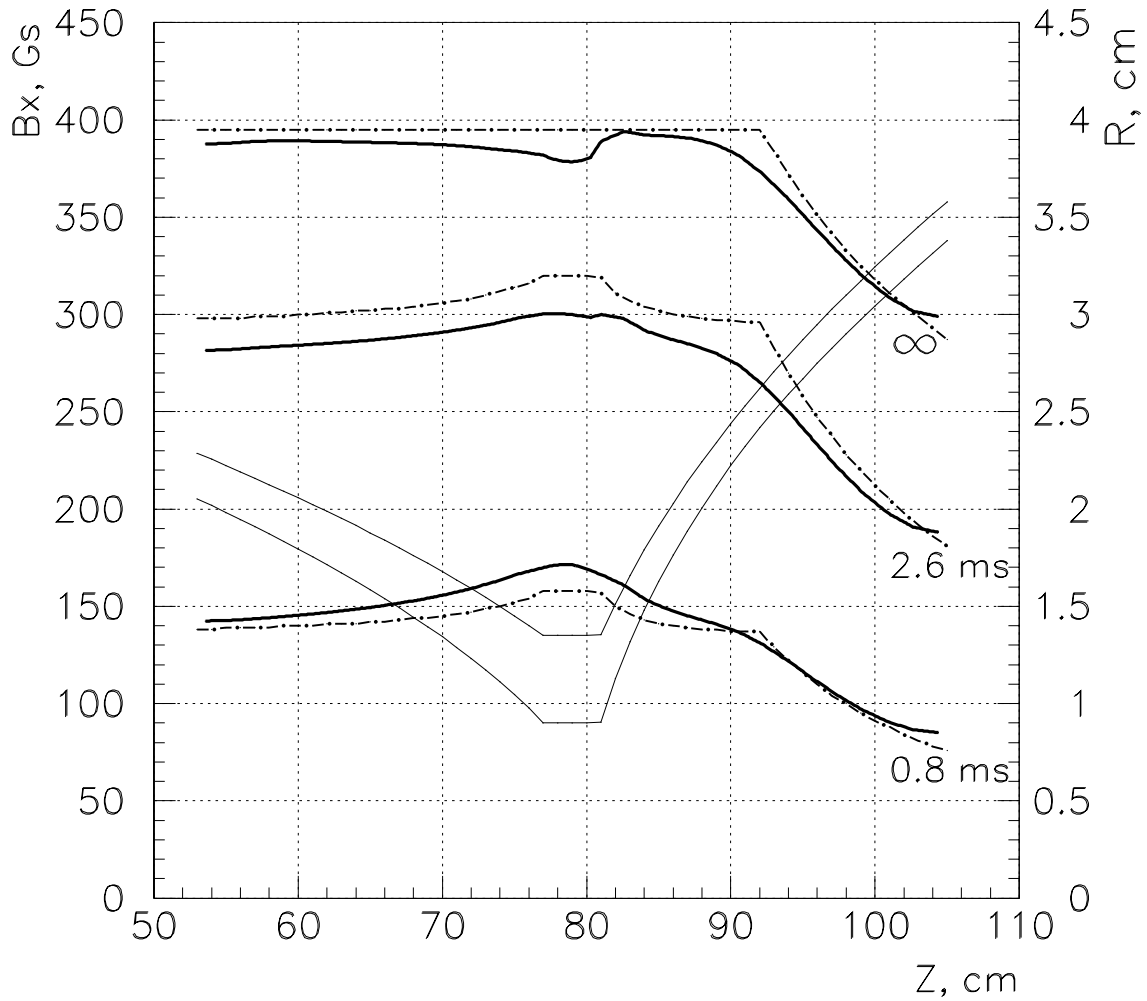
Figure 2.8: The magnetic field inside the central part of the inner conductor for the 2.6 ms and 0.8 ms pulse duration of a feeding current in comparison with that for the infinite pulse duration. Dash-dot lines were obtained with help of Expressions 1 and 3.
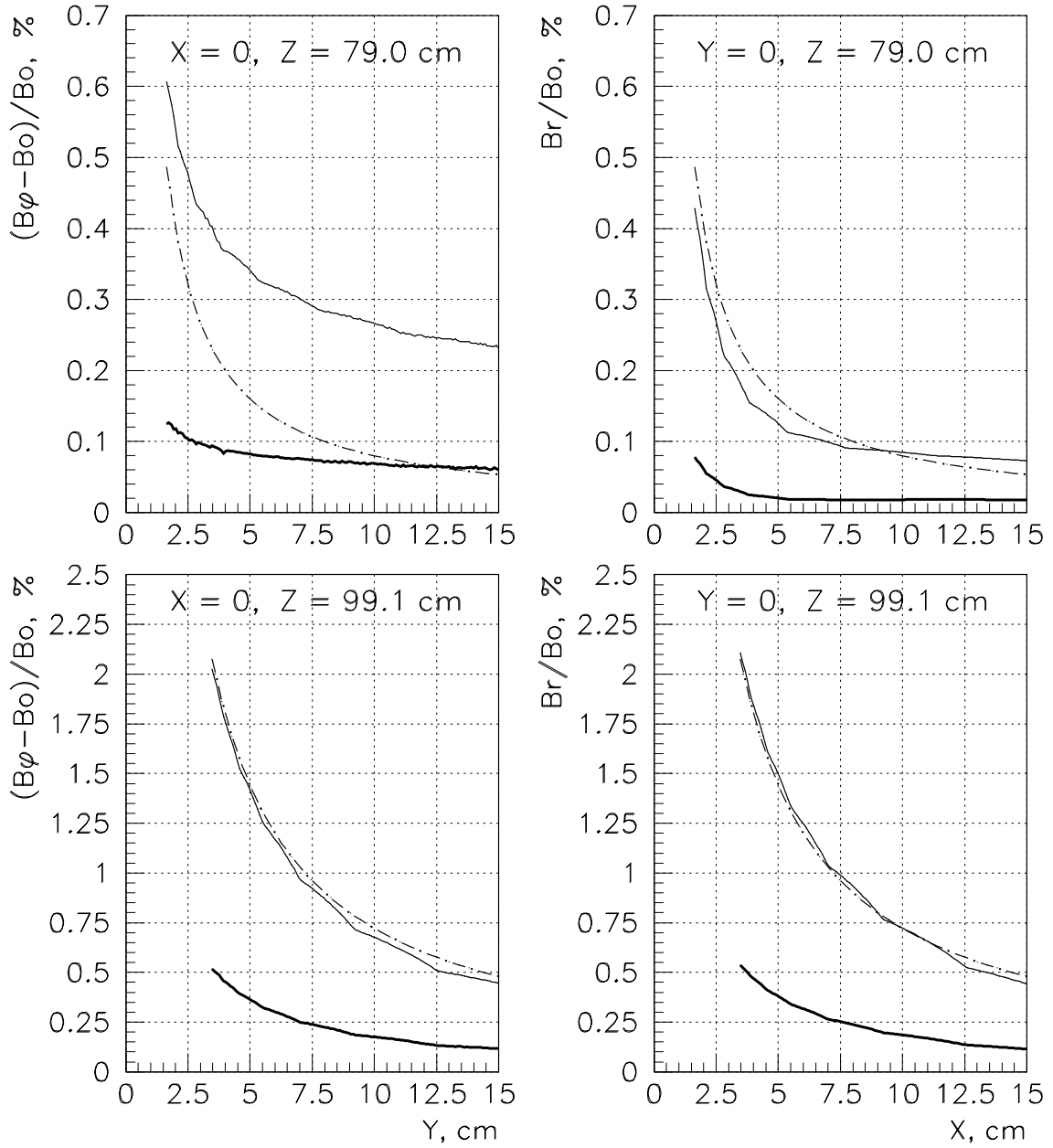
15

Figure 2.9: Deviations of the toroidal magnetic field from its nominal value due to the 0.1 mm eccentricity of the inner conductor for the 0.8 ms pulse duration of a feeding current (thick lines) in comparison with those for the infinite pulse duration. Dash-dot lines were obtained with help of Expression 2.
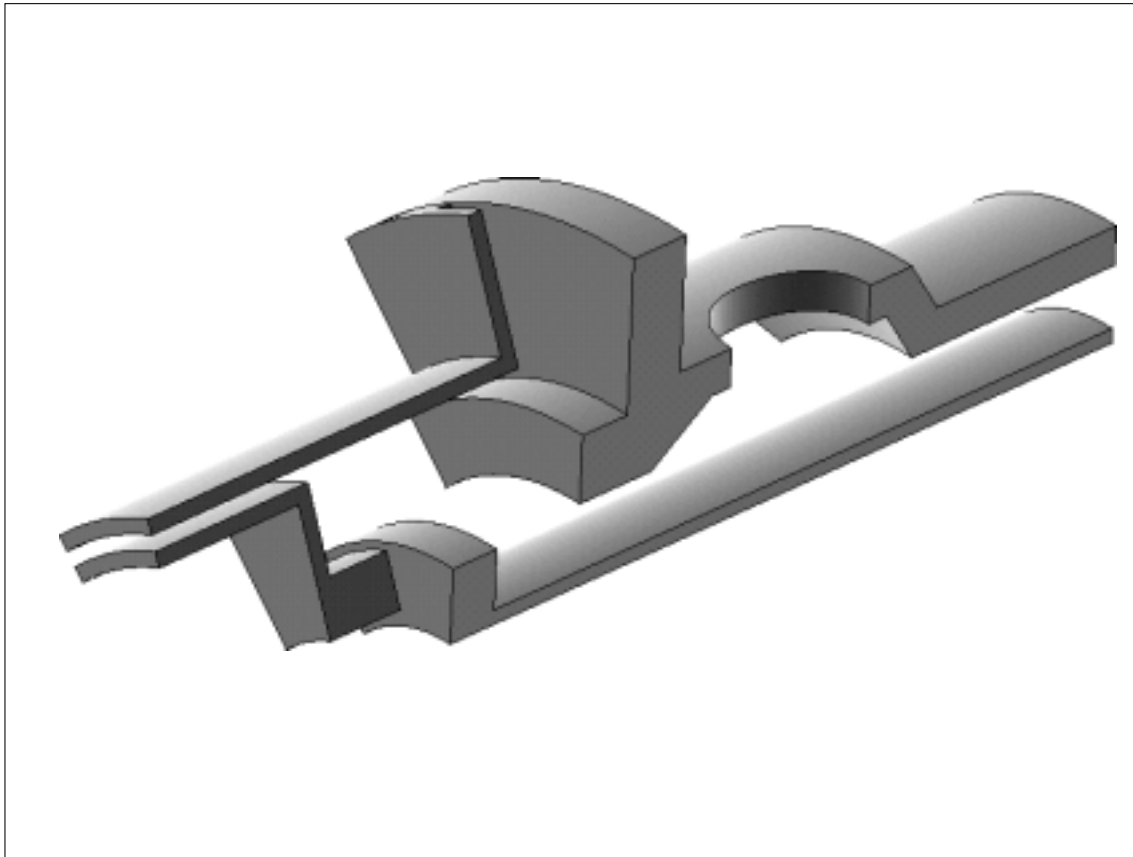
Figure 2.10: The ANSYS model for calculations of the magnetic field at the downstream end of horn.
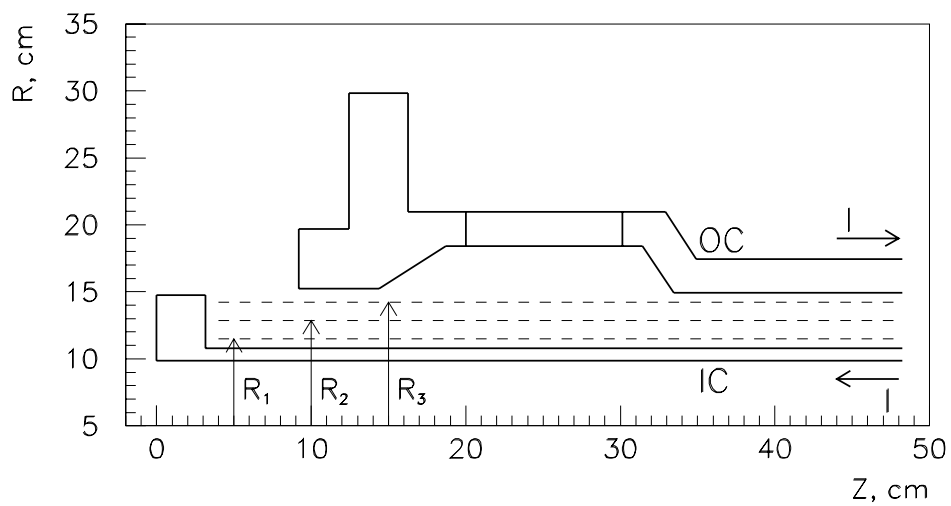

Figure 2.11: To calculations of the magnetic field at the downstream end of horn. $R_1 = 11.48$ cm, $R_2 = 12.86$ cm, $R_3 = 14.23$ cm.
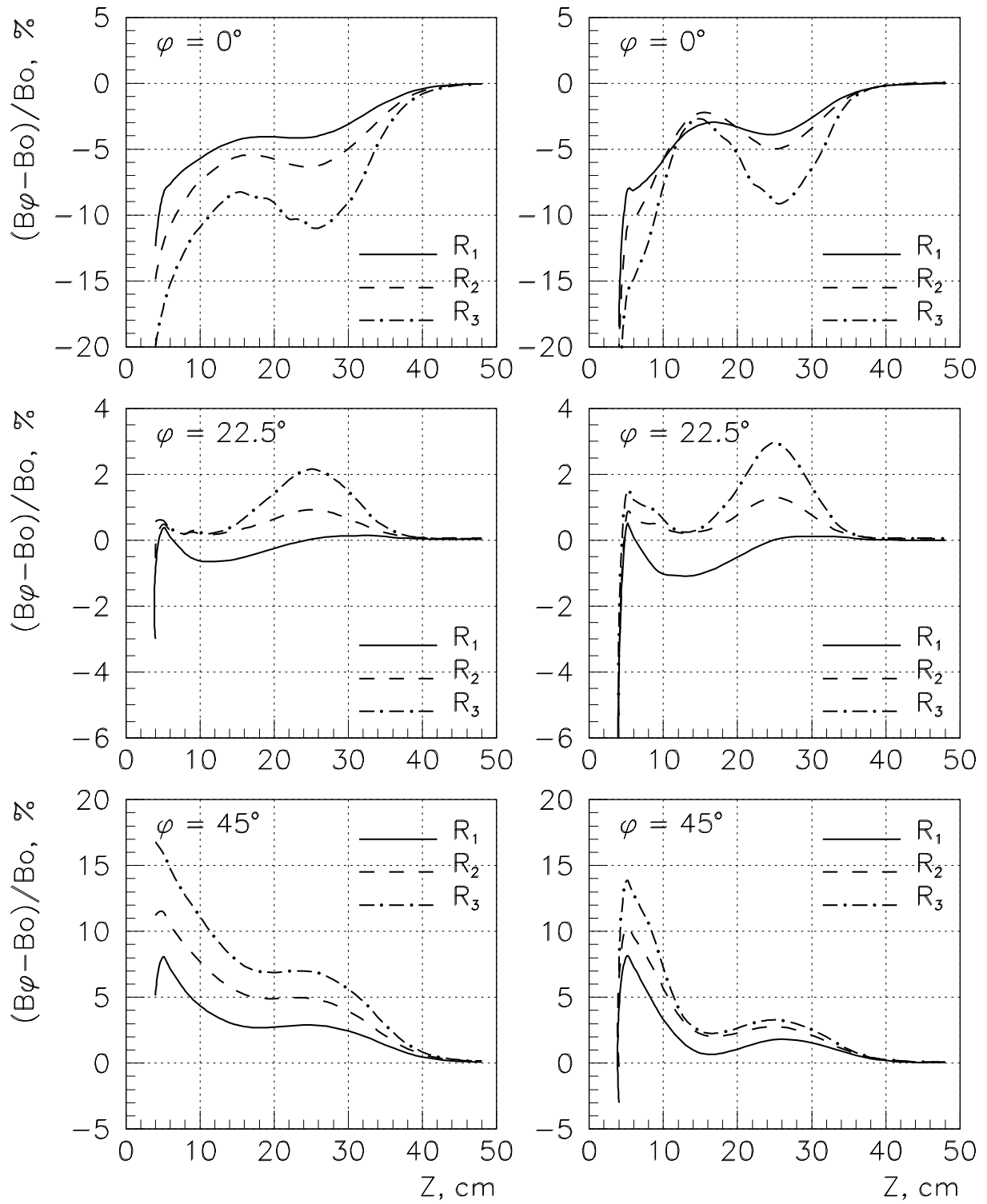
Figure 2.12a: Deviations of the toroidal magnetic field B_φ from its nominal value B_0 at the downstream end of horn for the infinite (left) and 0.8 ms (right) pulse duration of a feeding current.

Figure 2.12b: Deviations of the toroidal magnetic field B_φ from its nominal value B_0 at the downstream end of horn for the infinite (left) and 0.8 ms (right) pulse duration of a feeding current.
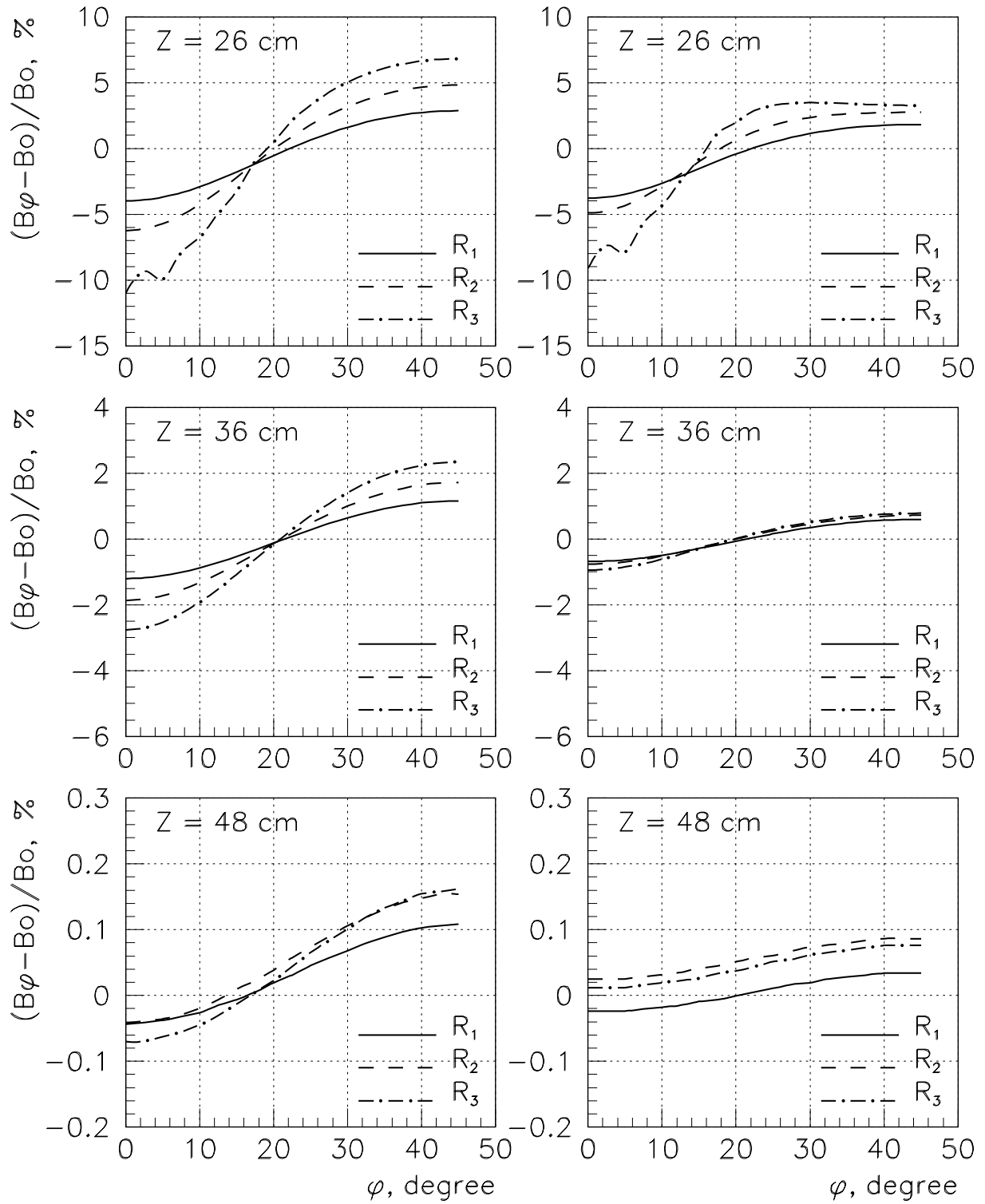
19

3   Hardware for Magnetic Field Measurements

To construct the hardware for magnetic measurements, the Hall probe was chosen as the element sensitive to the magnetic field. Using of Hall probes allows:

- to arrange easy point-to-point 3-dimensional measurements of the magnetic field by mounting probes in three sides of a rectangular rod;

- to see directly the magnetic field by measuring Hall voltages in two opposite directions of the operating current of the probe. In this case the possible parasitic signal will be subtracted, as well as the pedestal of the ADC used for measuring of the Hall voltage.

Constructed hardware for magnetic measurements consists of:

- Calibrated Hall probes, the precision radial moving arm and linear transducer for measurements of probe movements, which mounts with help of the support frame to the three probe holes in the outer conductor. This is used to measure the field between the inner and outer conductor as function of the radius.

- The calibrated 3-D Hall probe and a long support arm of variable length for mapping the region inside the inner conductor.

- The ADC for measurements of the pulsed Hall voltage, and required software driver for it, so that it can be read by LABVIEW on PC.

- The direct current source for Hall probes.

- Calibrated Hall probes for the measurement of current difference between strip-line pairs.

3.1   Hall Probes

3.1.1   Typical Parameters

The typical parameters of used Hall probes are given in Table 3.1. Used Hall probes have a very low temperature coefficient of the Hall voltage. It is very convenient for accurate absolute measurements of the magnetic field without temperature stabilization, which is practically impossible in

the case of magnetic measurements in the horn. The low sensitivity may be overcome with the coefficient of amplification of the ADC instrumental amplifier.

Dimensions, mm×mm×mm	$3 \times 3 \times 0.6$
Dimensions of sensitive area, mm×mm	1.5×0.5
Input resistance, Ohm	3.5–3.7
Output resistance, Ohm	5–5.5
Maximum power with heat-sink cooling, mW	150
Nominal operating current, mA	100
Residual voltage, μV	1–6
Sensitivity, mV/kGs	6.5–7.2
Temperature coefficient of the Hall voltage, %/K	–(0.001–0.005)
Temperature coefficient of the residual voltage, μV/K	–0.03
Coefficient of linearity at 20 kGs, %	–(0.79–0.95)
Coefficient of divergency, %	–(0.3–0.8)
Operating temperature range, K	1.5–373
Upper limit of the measured magnetic field, kGs	100

Table 3.1. Typical parameters of the ПХE602.817B Hall probe.

3.1.2 Calibration

Because the coefficient of the linearity is about 1%, each Hall probe was calibrated by nuclear magnetic resonance in the field range from –22.5 to +22.5 kGs for positive and negative directions of an operating current of the Hall probe[4]. The necessity of calibration at the negative field is derived from inequality to zero of the coefficient of divergency.

The measured magnetic field was recalculated using the cubic spline interpolation of the calibrated curve $B = f(V)$, where $V = (V_+ - V_-)/2$, V_+ and V_- are measured Hall voltages for positive and negative directions of an operating current.

---

[4]The maximal value of the magnetic field for the Hall probe calibration was chosen taking into account the value of field achievable at the minimal allowable distance of the Hall probe from the neck at the horn current 200 kA (see also Section 3.3).

3.1.3 Measuring Heads

The 3-D measuring head was constructed by mounting Hall probes with help of glue on sides of the ceramic rectangular rod (see Figure 3.1). The value of the thermal expansion coefficient is the same for the bottom layer of the Hall probe, ceramic and glue to minimize any forces on the probes. Hall probes of the 3-D measuring head were connected in series by operating current. To minimize the parasitic signal when measuring the pulsed field, pairs of current and voltage probe wires (0.05 mm in diameter) were twisted with 10 twists per 1 cm. The length of twisted wires 30 cm was chosen, because it was enough to provide connection of these wires to cable outside of horn when measuring the field between the inner and outer conductor.

Besides of the 3-D measuring head, which was used for field mapping inside the inner conductor, the 2-D measuring head (without the probe on the lateral side of the ceramic rod) was used for measurements of the field between the inner and outer conductor. For measurements of the field inside the strip-line, the Hall probe was mounted on the front side of the ceramic rod.

3.1.4 Measurements of the Hall Voltage

The Hall voltage was measured by the ADC card inserted into the PC ISA slot. The ADC card has eight differential inputs connected via programmable switches to the full instrumental amplifier with variable coefficient of amplification, the 16-bit ADC type AD977, the pulse quartz generator with programmable frequency and the external trigger. The minimum conversion time of the ADC is about 10 μs which allows to provide 85 measurements during the 850 μs current pulse. The coefficient of amplification of the ADC instrumental amplifier was chosen in such a way ($\sim$51) that one ADC count was corresponded to approximately 1 Gs. The statistical accuracy of the field measurement equal to about $\pm$2 Gs was defined by the ADC pulse to pulse accuracy ($\pm$2 counts).

3.2 Direct Current Sources for Hall Probes

Two DC sources were constructed to provide the operating current of Hall probes for measurements of the horn field (first one) and for measurements of the field between strip-line pairs (second one). Both current sources are the same by the operation. Integrated circuit AD780 is used as a high

precision reference voltage for the operational amplifier OP-37 with 100% negative feedback. The feedback signal is formed in the output current cascade made with the IRF830 insulated-gate field effect transistor. Frequency correction of the operational amplifier was chosen to provide its stable operation in the maximum frequency band as a necessary condition for measurements of the pulsed field.

Up to 20 Hall probes connected in series can be supplied with operating current by each current source without changing in its output characteristics. The measured current stability, in 20 minutes after switching on, was not lower than 10^{-5} in a temperature range (15–40)°C. The direction of the current may be controlled by the external TTL trigger.

3.3 Setup for the Measurements of the Field between the Inner and Outer Conductor

The setup for the measurements of the field between the inner and outer conductor and its fitting to the field probe holes in the horn outer conductor are shown in Figure 3.2. Figure 3.3 shows more detailed view of some parts of this setup.

The unit for movements of the probe is placed on the fiber glass plate clamped to the prism, which is fixed on the outer conductor by two clamps. It consists of two slide-ways fixed on the aluminum alloy support and the carriage with a nut. High accuracy finished contact surfaces of slide-ways and the carriage were machined out with help of grinding machine. The carriage is driven by a screw. The measuring head with the 2-D Hall probe is attached to the carriage as it is shown in Figure 3.3. It is protected from the water sprayed on the inner conductor with help of the fiber glass pipe.

The sizes of setup are chosen in such a way that the Hall probe is moved along the line crossing the horn axis on measuring the B_φ component of the field. Because the minimum distance between the external surface of the neck and the geometrical center of this Hall probe is approximately equal to 6 mm, it limits the measured field by the value of $\sim$22.5 kGs under the horn current of 200 kA. As measurements show, the transverse displacement of the Hall probe during its movement at the distance equal to 200 mm was not exceeded a few microns. It may be neglected at B_φ measurements because the relative error $\delta B_\varphi / B_\varphi \simeq (\delta x / r)^2$, where δx is the transverse displacement of Hall probe, r is the radius of measurement.

The another Hall probe is located 2.35 mm away from the direction of movements (as it is shown in Figure 3.4) and can measure B_y component of the field (Y-axis coincides with the direction of movements).

The measurements of movements of the Hall probe are carried out with help of the LS403 linear transducer with resolution of 1 μm and the block of indication VRZ460 (HEIDENHEIN, Germany) connected to PC via the RS-232 interface.

3.4 Support Arm with the 3-D Hall Probe for Mapping the Region inside the Inner Conductor

The 3-D Hall probe for mapping the region inside the inner conductor was mounted at the end of the long support arm of variable length. It is a telescopic type arm with lengths of its parts equal to 3130, 2165.5 and 1210 mm for measurements in the downstream (long) part and 1050 mm for measurements in the upstream (short) part of the horn. The arm is made of an insulated material. Its resistance to the ground is not less than 1 GOhm at the voltage 500 V. The cable with twisted pairs in the aluminum screen passes inside the arm. The sag of support arm was compensated by variation of the angle in the point of its attachment to the 3-D machine with help of the micrometer screw, as it is shown schematically in Figure 3.5. The counts of the micrometer screw for different arm lengths are given in Table 3.2.

Length of the arm, mm	Micrometer counts
1050	4.455
1210	4.72
2165.5	5.75
3130	8.30

Table 3.2. Counts of the micrometer screw for different arm lengths.

3.5 Measurements of the Horn Current

The setup for measurements of the difference of currents in strip-line pairs is shown in Figure 3.6. Its operation is based on measurements of the magnetic field between pair of conductors by calibrated Hall probes mounted on the fiber glass support and inserted in the center of the strip-line.

ANSYS calculations show, that at the 850 μs sine-wave current with the amplitude of 50 kA in each pair of conductors and following directions of currents in the conductors $(-++--++-)$, the magnetic field is $B_1 = -B_4 = 1945.0$ Gs and $B_3 = -B_2 = 1988.0$ Gs. Enumeration of pairs is given in Figure 3.6. The partial derivatives $C_{ij} = \partial B_i / \partial I_j$, where B_i is the field in pair i and I_j is the current in pair j are given in Table 3.3.

I_j	C_{1j}	C_{2j}	C_{3j}	C_{4j}
I_1	37.56	1.64	-1.0	0.64
I_2	1.64	37.4	1.72	-1.0

Table 3.3. Partial derivatives of the field (Gs/kA) with respect to current in pairs of the strip-line.

The measurements of difference of currents in strip-line pairs was not carried out at the first stage of field mapping. Instead it, there were carried out direct measurements of currents with help of current transducers, installed in the horn power supply, by measuring their output voltage (9 times attenuated) by the ADC, similar to described above.
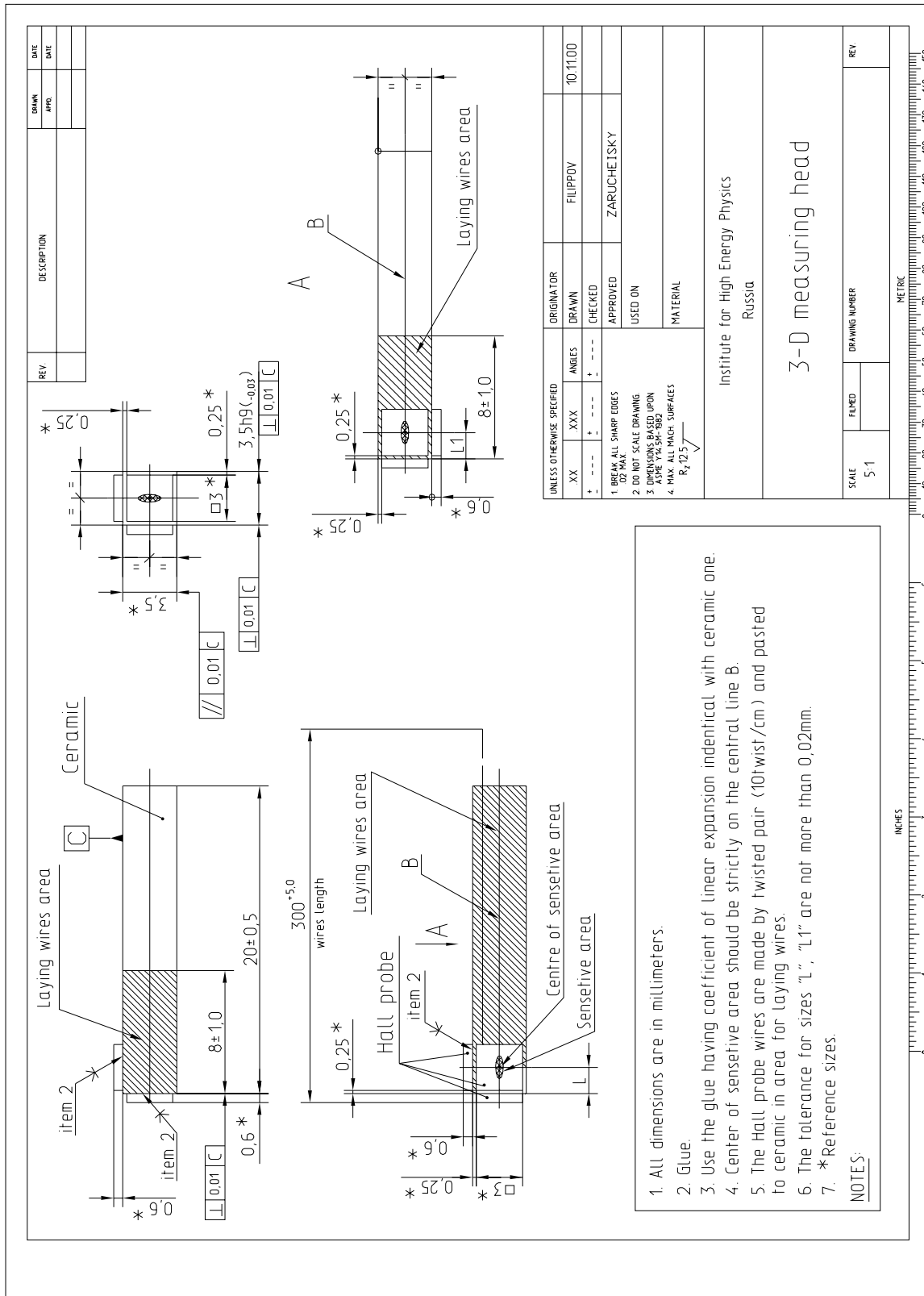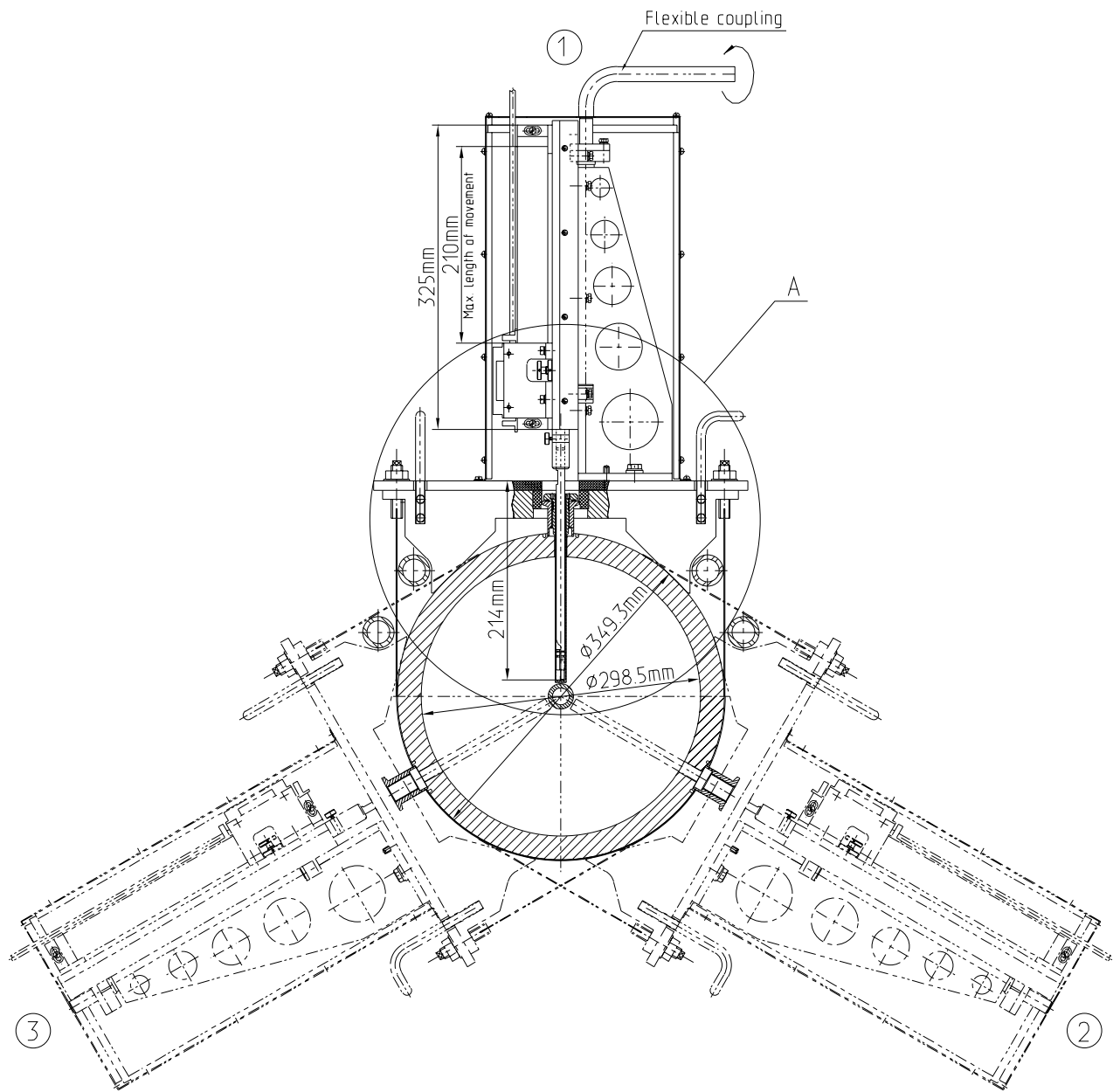
Figure 3.1: The 3-D measuring head.

Figure 3.2: The setup for measurements of the magnetic field between the inner and outer conductor. Digits in circles correspond to positions of the setup as viewed from the strip-line.
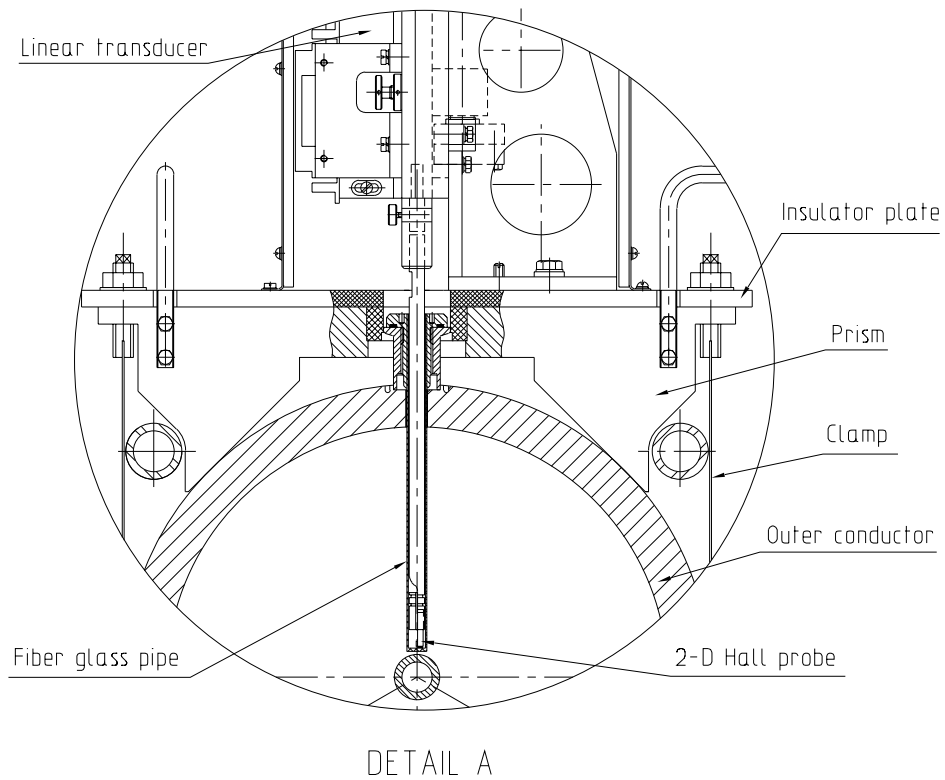
DETAIL A

Figure 3.3: Some details of the setup for measurements of the magnetic field between the inner and outer conductor.
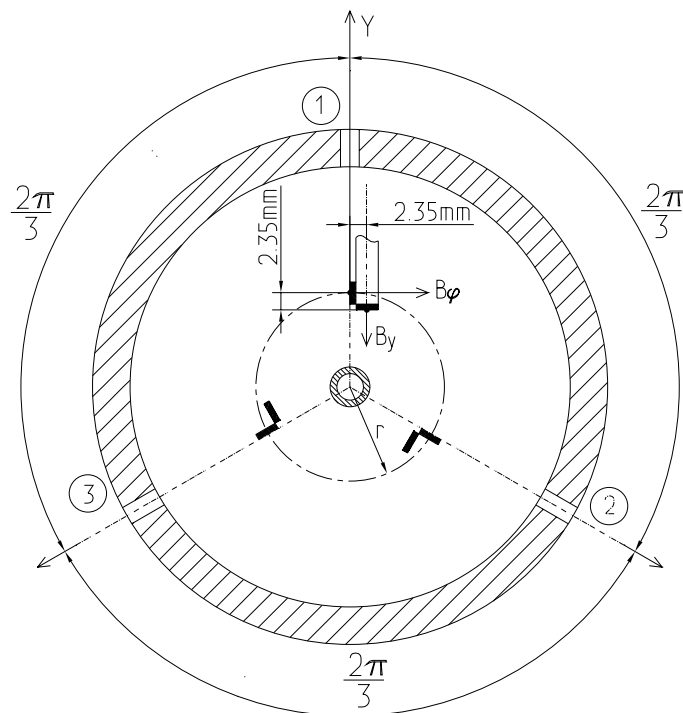

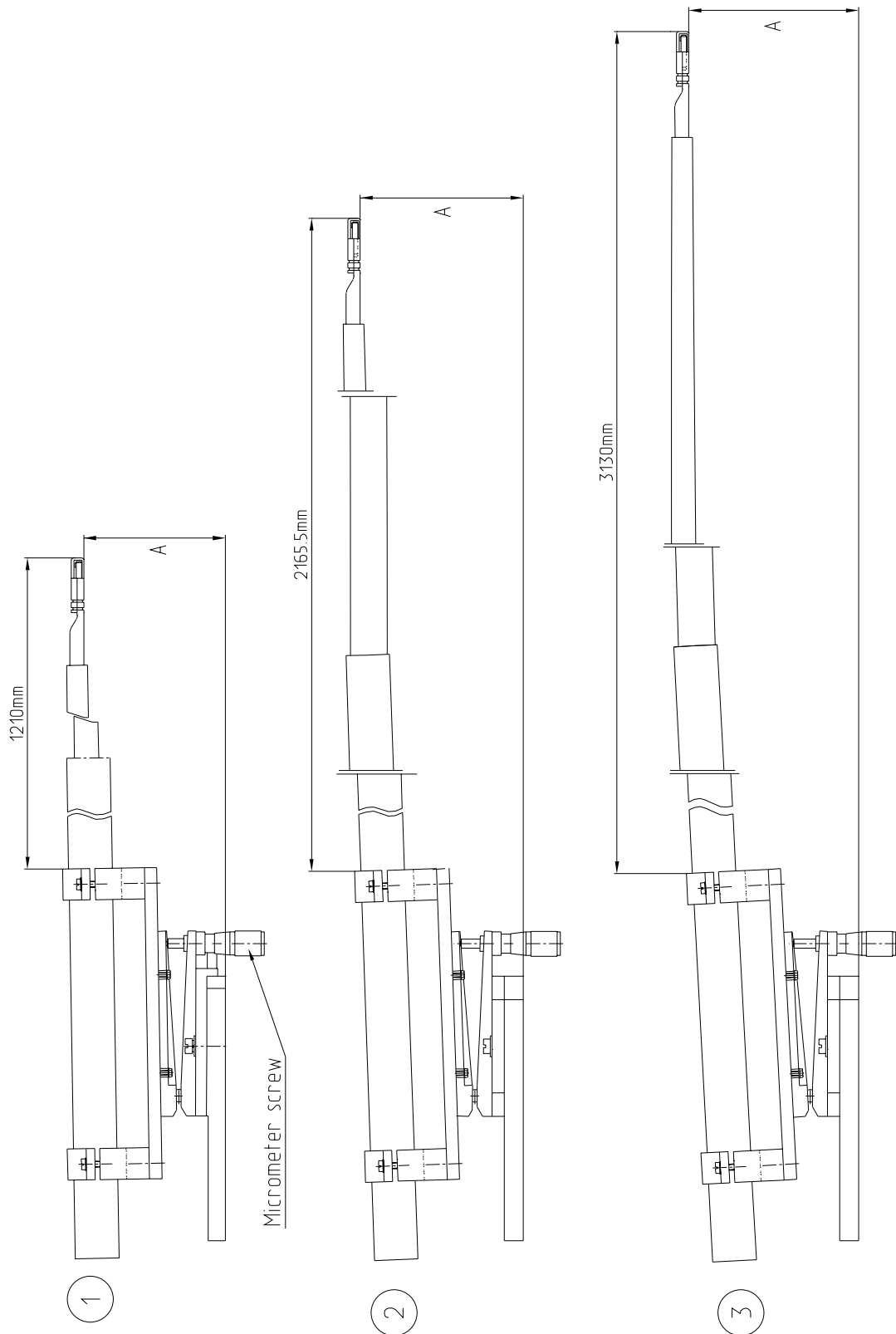Figure 3.4: The schematic view of Hall probes location.
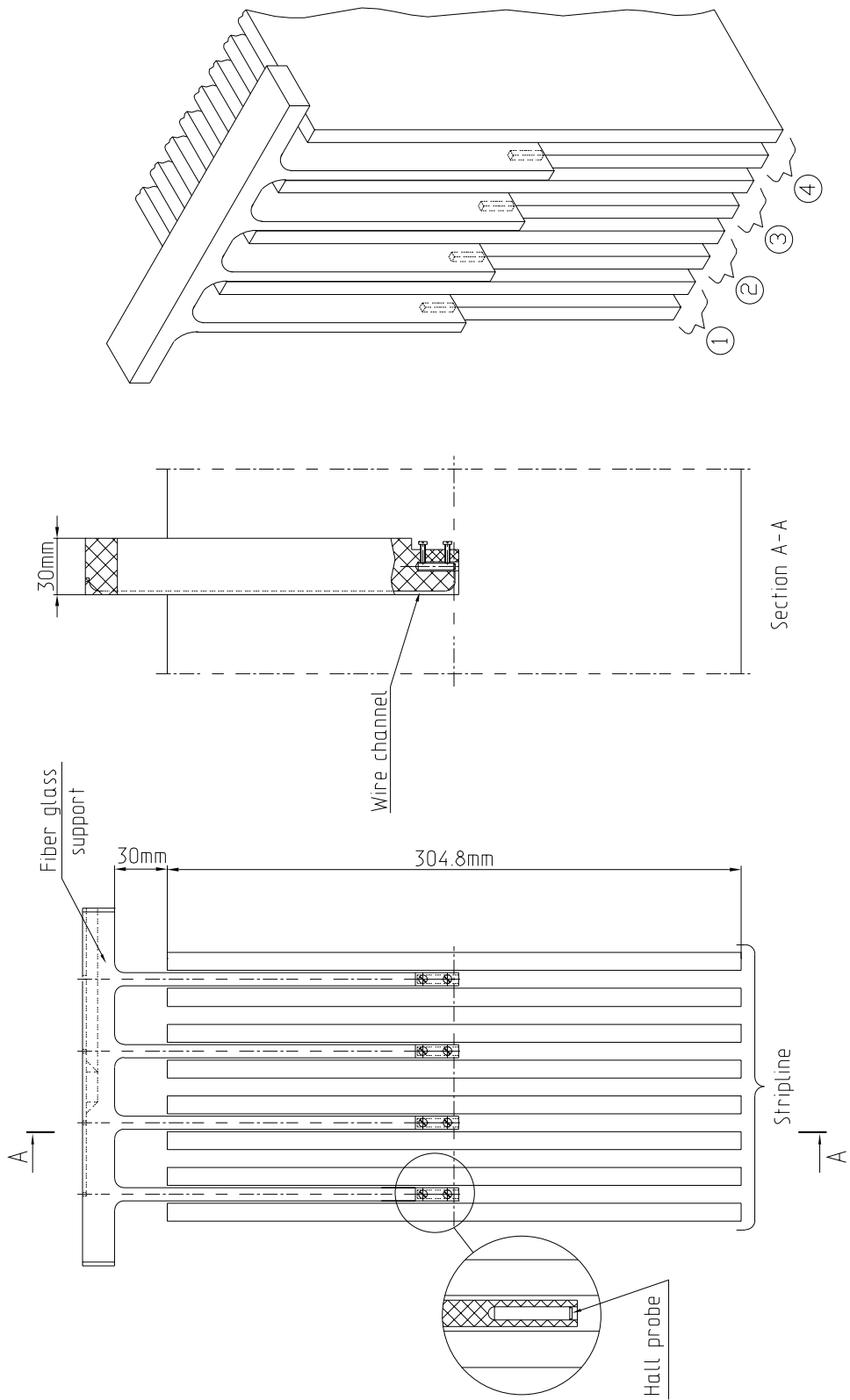
Figure 3.5: The compensation of the arm sag.

Figure 3.6: The setup for measurements of a difference in currents in stripline pairs.

4 Results of Magnetic Measurements

The measurement of magnetic field in each point were produced for two pulses of horn current: the first measurement — for positive direction of the Hall operating current and the second one — for the inverse direction. The measured magnetic field was normalized to the nominal current I_0 via relation $I_0/(I_+ + I_-)/2$, where I_+ and I_- are measured currents for positive and negative directions of the Hall operating current.

4.1 Magnetic Field between the Inner and Outer Conductor

The magnetic field between the inner and outer conductor was measured at current amplitude $I_0 = 150$ kA of sine-wave pulse with duration 850 μs and repetition period 16 s.

The main problem in processing of measured data of the field between the inner and outer conductor is conversion of data, received by the linear transducer, to the radius of the Hall position counted from the neck axis. This conversion was made, fitting the data by the formula: $B_{\varphi i} = \mu_0 I_0 / 2\pi (R_i + A_i)$, where $B_{\varphi i}$ is the measured field for i position ($i = 1, 2, 3$) of the measuring setup (see Figure 3.2), R_i is the data from the linear transducer in position i, A_i is constant which should be defined after fitting, μ_0 is the permeability of free space. This approximation does not take into account the possible error in the measurements of the horn current, but gives the values for A_i which practically do not depend on the number of fitting points: $A_1 = 185.639$ mm, $A_2 = 185.978$ mm and $A_3 = 185.518$ mm. The difference $\Delta A_{13} = A_1 - A_3 = 0.121$ mm and $\Delta A_{23} = A_2 - A_3 = 0.460$ mm are agree well with measured values $\Delta A_{13}^{meas} = 0.110$ mm and $\Delta A_{23}^{meas} = 0.405$ mm[5]. Fitting of measured data by the formula $B_{\varphi i} = k_i \mu_0 I_0 / 2\pi (R_i + A_i)$, where k_i is the coefficient depended on the accuracy of current measurements, gives the possible error in the current measurements $\sim (2\text{–}3) \times 10^{-4}$ that may be neglected in the data processing.

The results of this data processing, where the distributions of measured focusing field are functions of the radius, are given in Figure 4.1. Deviations of measured field from the nominal value $B_0 = \mu_0 I_0 / 2\pi R$ for different

---

[5]Such measurements were made with help of the steel rod, mounted in the setup instead of the Hall measuring head, by touching to the neck surface.

positions of the measuring setup are given in Figure 4.2. As it follows from these plots, the deviation of the measured field from the nominal value does not exceed 0.1% for the radius $R \leq 8$ cm. For larger radius ($R \geq 8$ cm) the local perturbation of the magnetic field is caused by holes in the outer conductor.

The accuracy of B_y measurements strongly depends on the orientation of corresponding Hall probe mounted at the end of the ceramic rectangular rod, i.e. $B_y \simeq \widetilde{B_y} - B_\varphi \beta$, where $\widetilde{B_y}$ and B_φ are field components as measured by Hall probes, $\pi/2 + \beta$ is the orientation of Hall probe at the ceramic rod end with respect to the probe which measures the B_φ component. The processing of measured data for the B_y component shows that $\beta \simeq 0.007$. This was taken into account in comparison of measured components of the magnetic field with those calculated by the ANSYS code (see Figure 4.3). One can see from this Figure, that both measured field components are in a good agreement with calculated ones. Some difference ($\sim$10 Gs) between measured and calculated values of the B_y component at $y \leq 14$ cm may be explained by the accuracy of ANSYS calculations.

4.2 Magnetic Field inside the Inner Conductor

Measurements of the magnetic field inside the inner conductor were produced at the nominal current $I_0 = 200$ kA and repetition period 8 s. Initially, the field mapping was performed from the upstream horn end and after moving of the 3-D machine — from the downstream end.

Measurements scans from the upstream end were made for five positions of the support arm: central ($\Delta x = \Delta y = 0$) and four shifted ($\Delta x = \Delta y = \pm 2$ mm) positions, the scans from the downstream end — for central and two shifted ($\Delta x = \Delta y = +2$ mm) positions.

The distribution of the measured dipole field along the horn axis is given in Figure 4.4[6]. The dipole field inside the inner conductor does not exceed 34 Gs and exists only in a short region near the horn neck. Using results of ANSYS calculations of the dipole field arose inside the inner conductor due to the eccentricity between his inner and outer surfaces (see Section 2), one may estimate the value of the eccentricity equal about 0.02 mm.

---

[6]The longitudinal probe position is counted from the plane tangent to the rounded surface of the transition from the inner to outer conductor, X–axis is directed to the right as viewed from the strip-line, Y–axis to the upward.

The measured dipole field shows well places of welding of different parts of the horn inner conductor: transition from the inner to outer conductor with part A (peak in B_y at $Z = 14.6$ cm), part A with part B (peak in B_x and B_y at $Z \simeq 60$ cm) and part B with part C (peak in B_x at $Z \simeq 110$ cm).

After $Z \geq 150$ cm the B_x is practically invariable. Simple calculations give the average field for the region $Z \geq 150$ cm equal to ~ 3.5 Gs. It may be probably explained by the fact that at this region small horizontal component of stray field exists. It may be confirmed by measurements of the field at this region with a zero horn current.

Small transverse gradient of the magnetic field was detected in the region $180 \leq Z \leq 290$ cm (Figure 4.5). It confirms the ovality of the inner conductor arose during the welding process of parts D, E and F. But the value of the gradient may be estimated as 0.5–0.7 Gs/cm and may not be taking into account in calculations of the FAR/NEAR ratio.

In conclusion it should be pointed out, that given above results of magnetic measurements are in a good agreement with the expected horn fields and confirm high quality of the prototype horn construction.
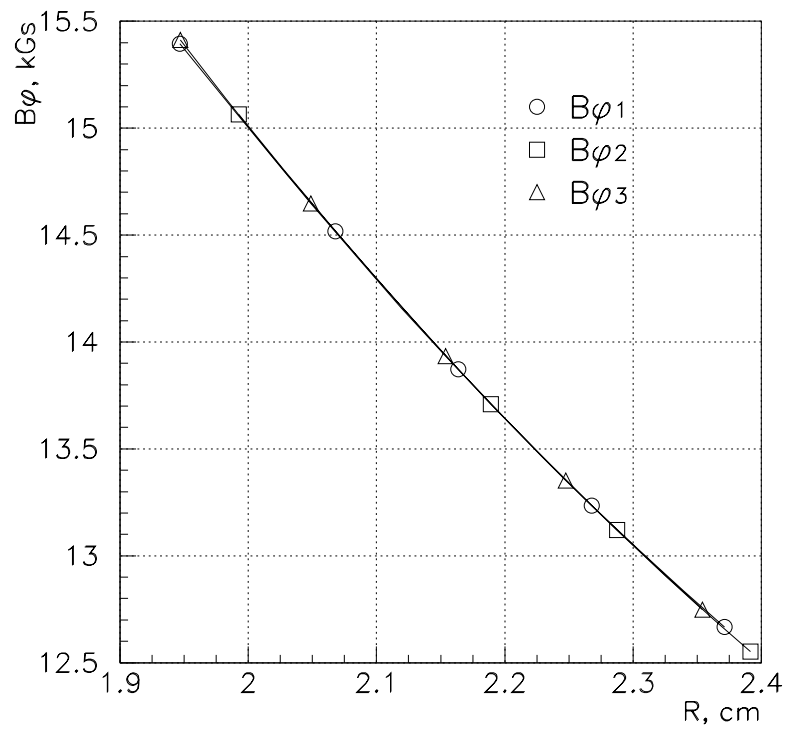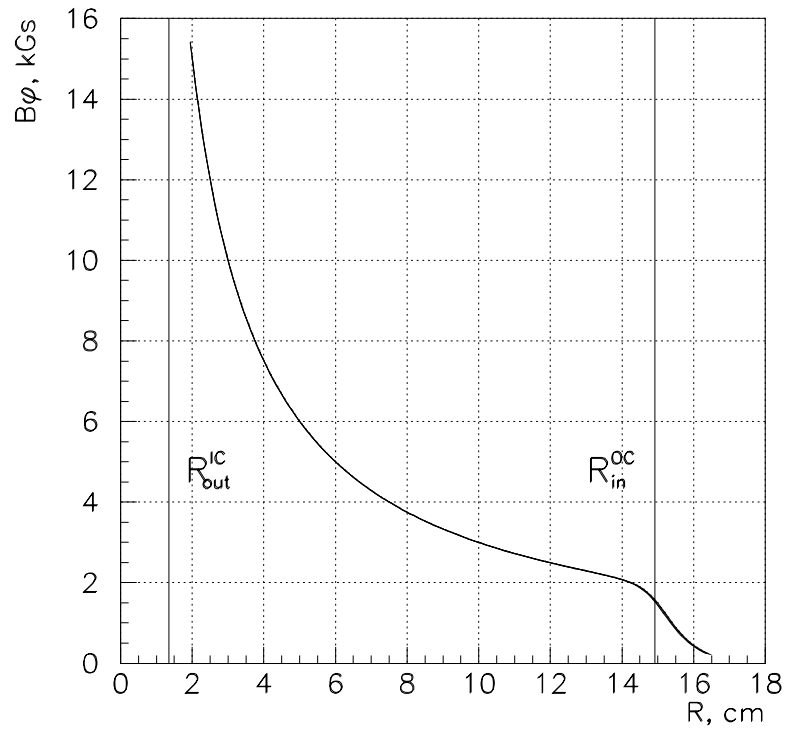
Figure 4.1: The measured magnetic field in the neck region of the prototype horn.
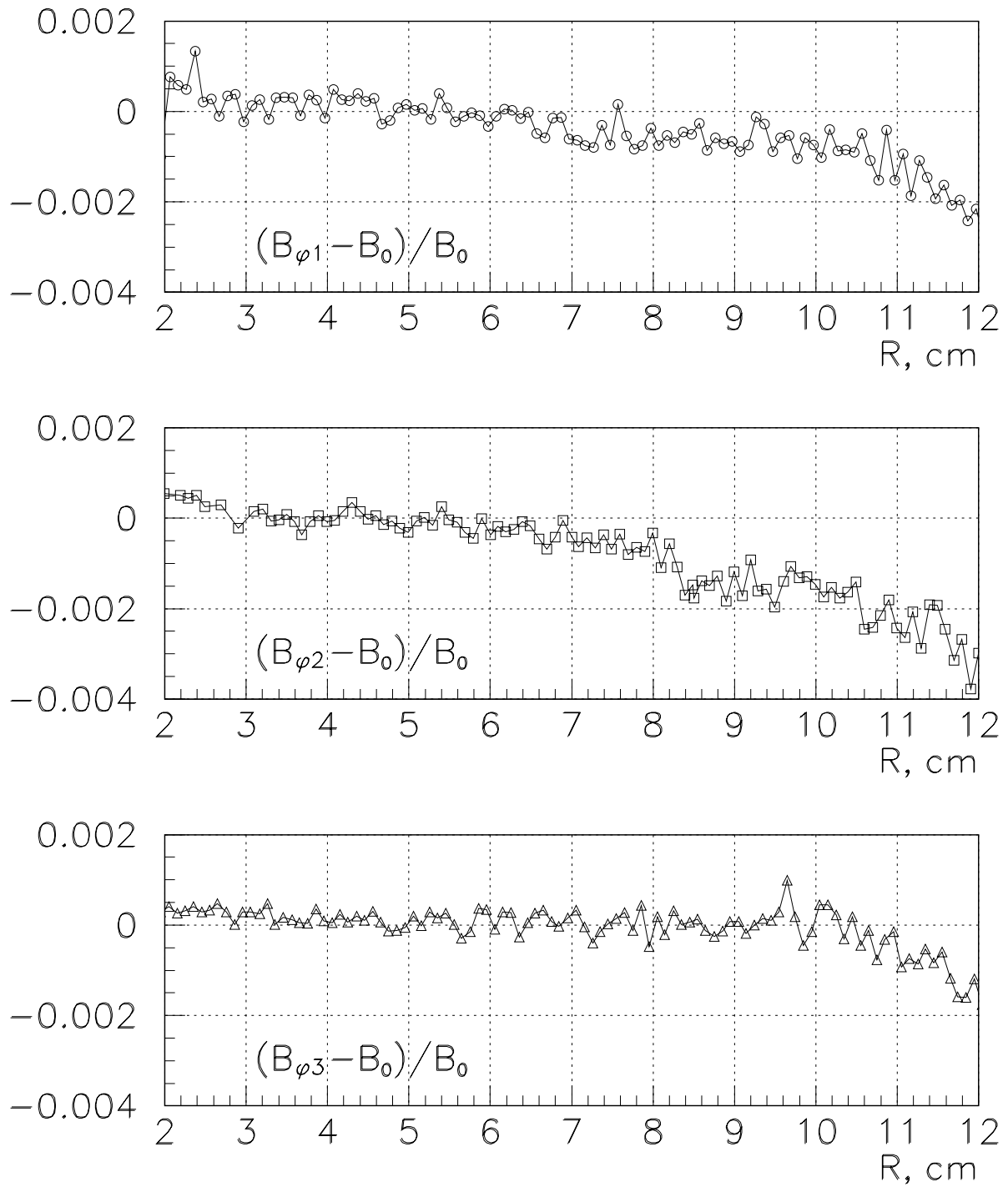
Figure 4.2: Deviations of the measured magnetic field B_φ from its nominal value B_0 in the neck region of the prototype horn.
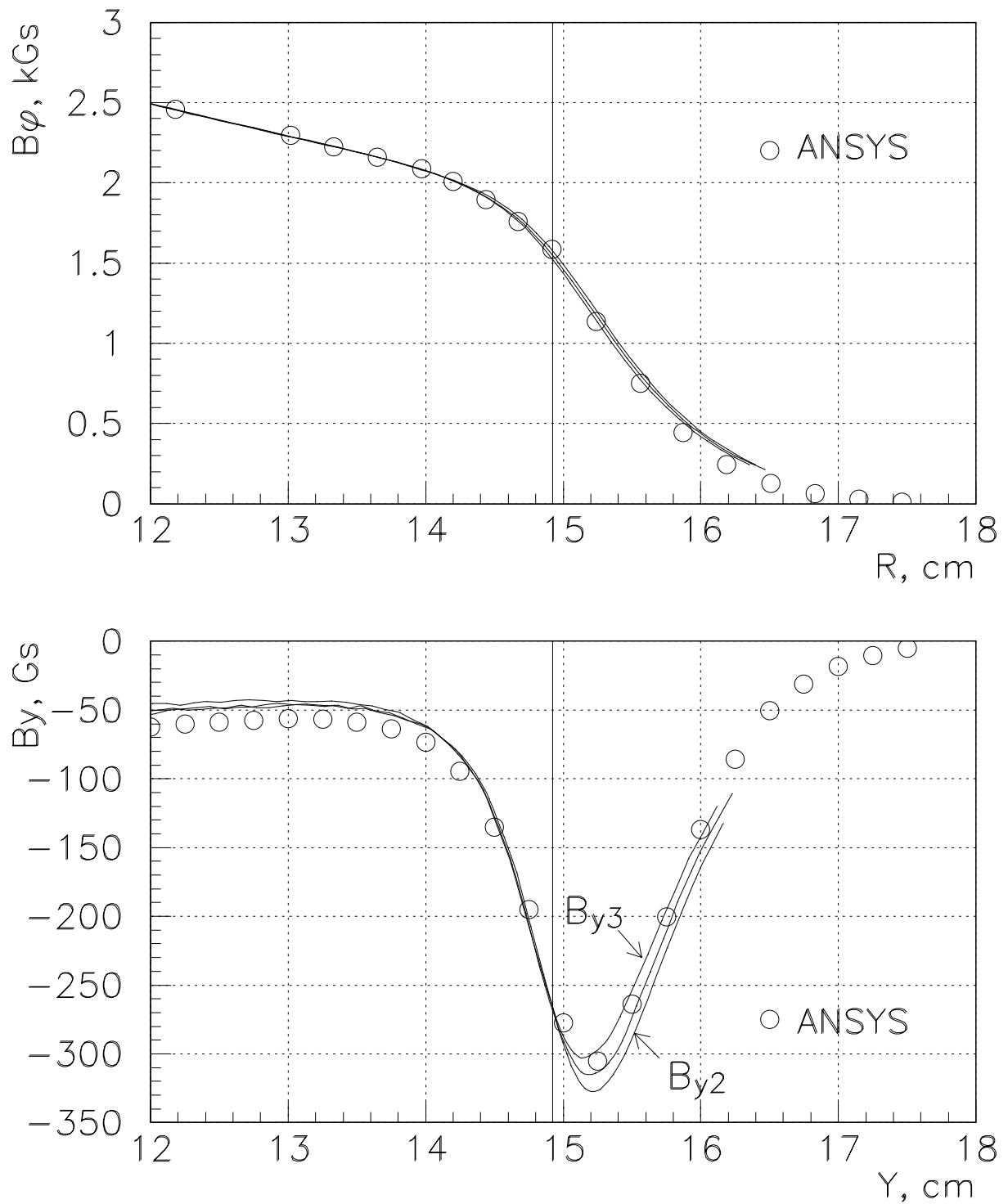
Figure 4.3: Measured components of the magnetic field in the neck region of the prototype horn in comparison with their calculated values. The B_y component was measured along the line coinciding with the axis of a measuring arm (see Section 3), i.e. 2.35 mm from the radial direction.
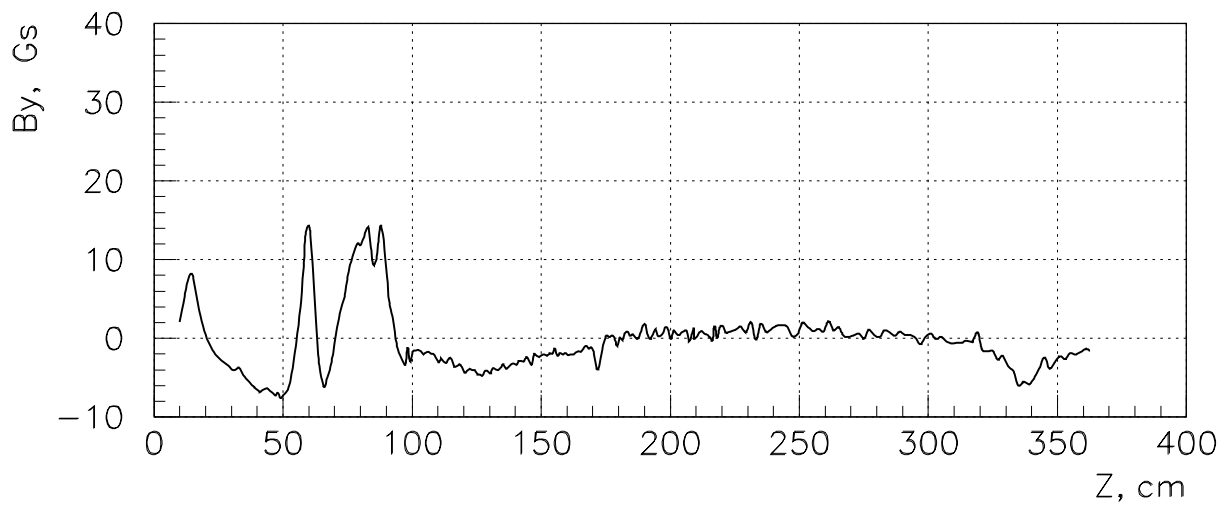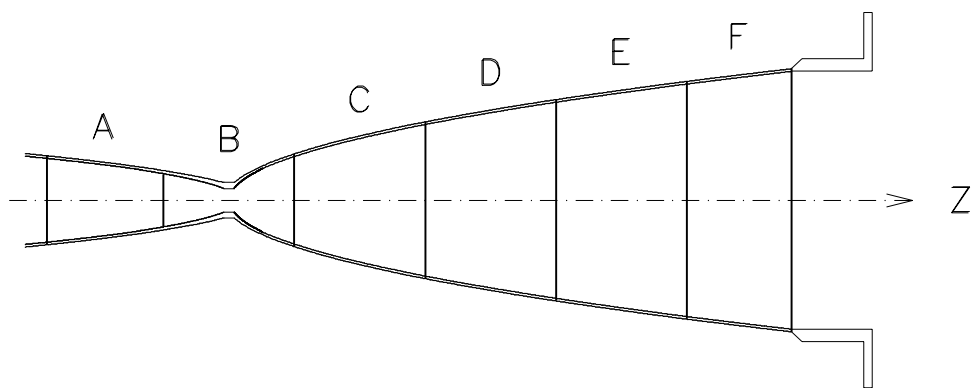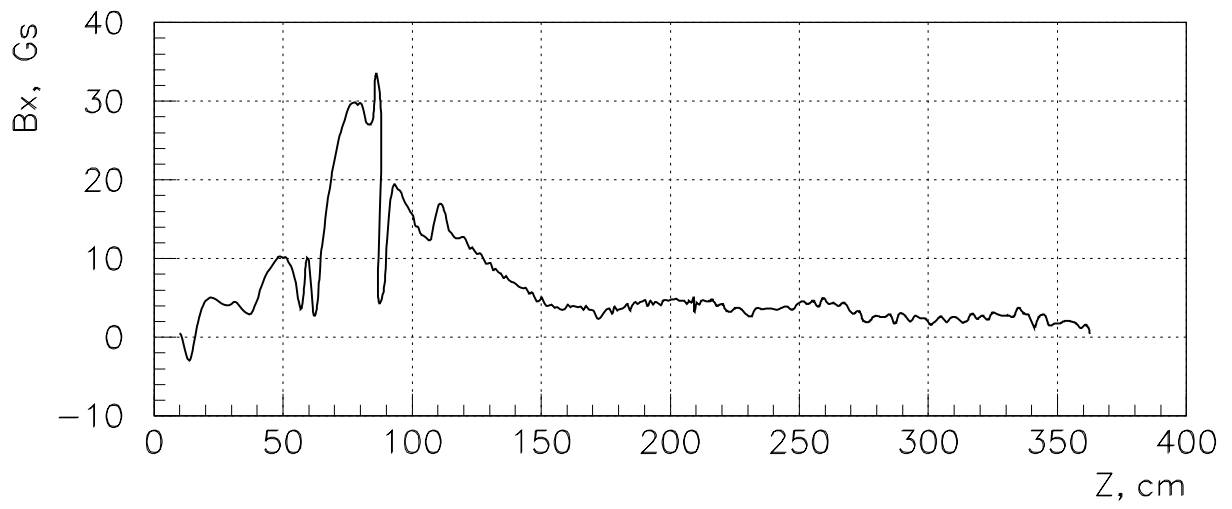
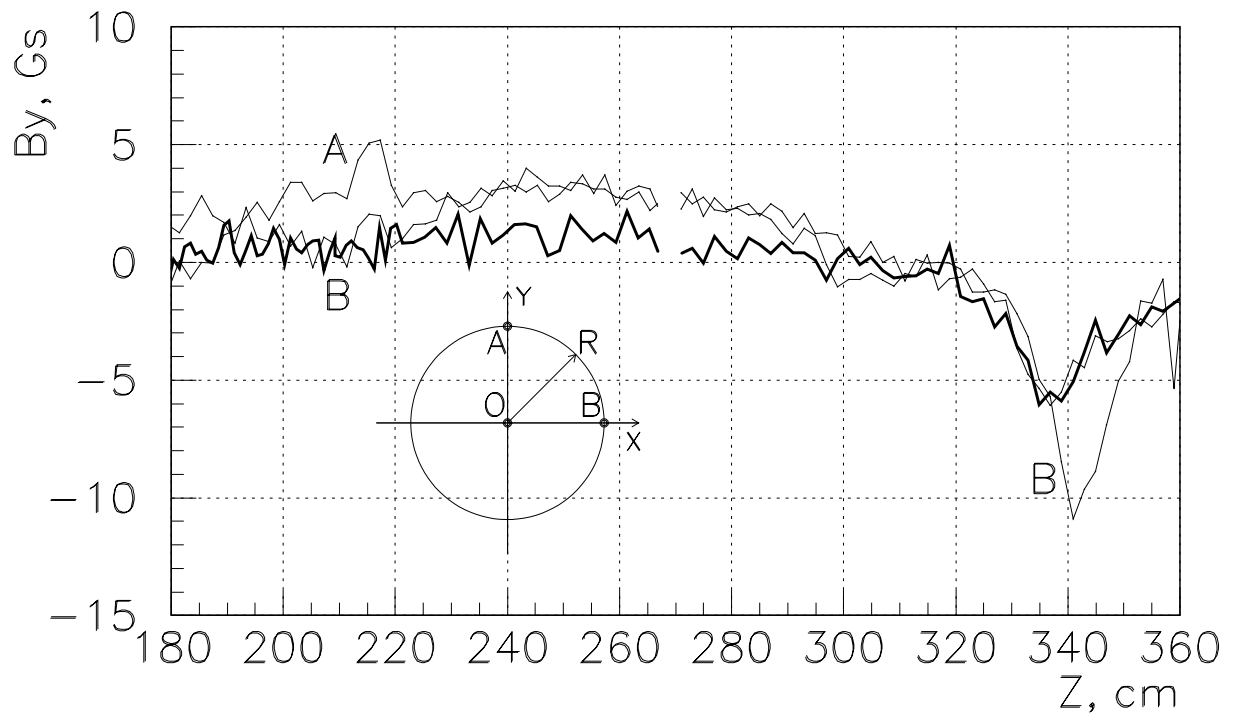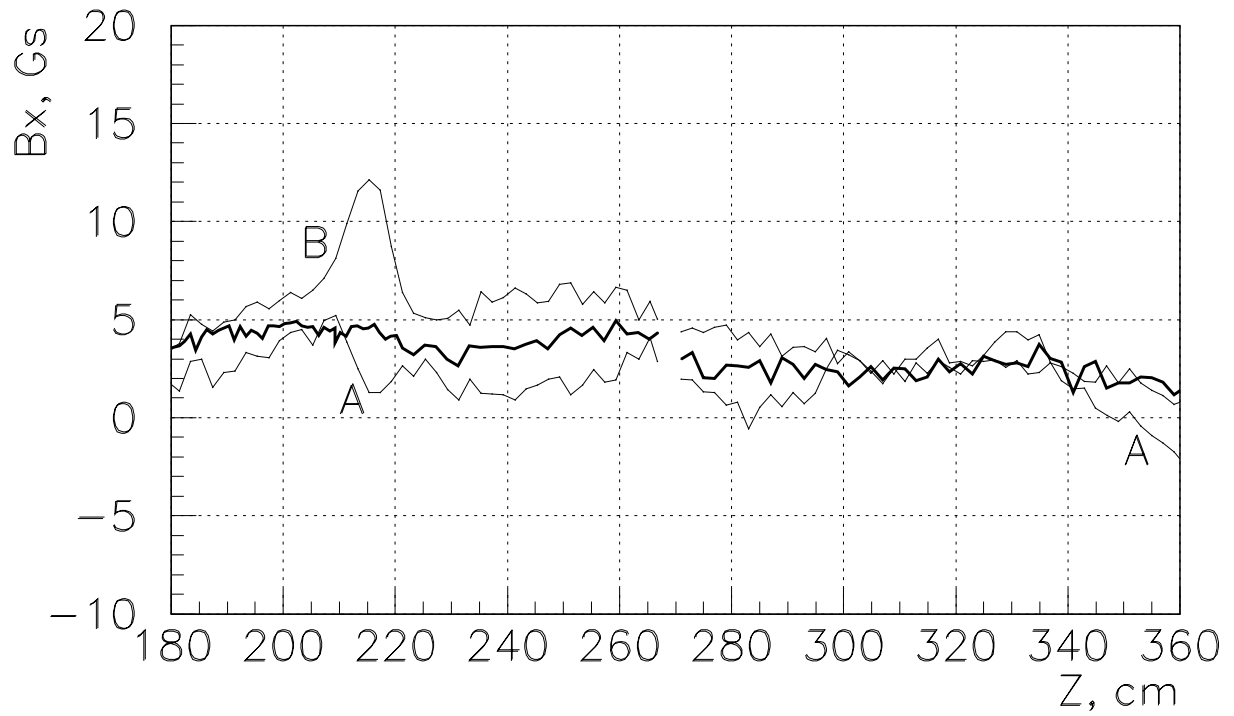Figure 4.4: The measured magnetic field at the axis of the inner conductor.

37

Figure 4.5: The measured magnetic field inside the inner conductor. The thick line gives the field at the axis of the inner conductor (Figure 4.4). Directions of X and Y axes are shown as viewed from the strip-line. $R = 40$ mm for $Z < 270$ cm and $R = 50$ mm for $Z > 270$ cm.